Microphase Separation of Block Polymers

By

Takeji HASHIMOTO, Mitsuhiro SHIBAYAMA, Mineo FUJIMURA, and Hiromichi KAWAI

(Received December 27, 1980)

Abstract

Block polymers composed of incompatible block chains of A and B undergo a microphase separation due to the repulsive interaction between A and B in solutions at concentrations above the critical concentration, or in bulk at temperatures below the critical temperature, T_c, (for the A-B system having an upper critical solution temperature) or above T_c (for the system having a lower critical temperature). The microphase separation results in a microdomain structure in solid state, the morphology of which controls the unique physical properties of the block polymer systems. This article reviews recent developments in the area of (i) microphase separation and phase-separated structure in solution and in bulk (ii) microdomain structure in solid state and (iii) polymer-polymer interphase in block polymers for amorphous and linear block polymer systems having simple architectures (e.g., polystyrene and polyisoprene or polystyrene and polybutadiene diblock or triblock polymers).

I. Scope

In section II we shall review the microphase separation in solutions and developments of the microphase-separated structure with increasing concentration. The phase separation will be shown to affect some optical properties and rheological properties of the solutions. We shall briefly describe a new and novel technique of small-angle X-ray scattering with a position sensitive detector as a method to characterize the phase separation and the phase-separated structure in the solutions.

In section III we shall discuss the microphase separation of block polymers in bulk. Here we review some theoretical background on critical temperature at which the phase separation will develop from the homogeneous mixture of A and B, on the morphology of the phase-separated microdomain structure (size, shape, spatial distribution of the domains), and on the structure of the boundary region ("interphase") between A and B domains. These aspects of the phase separation

Department of Polymer Chemistry

in bulk are described as a function of molecular parameters such as molecular weight, chemical composition, density and the interaction parameter between A and B. Also described are the thermodynamic variables such as temperature in terms of equilibrium theories developed on the basis of random flight chain statistics in a confined space. The statistics demand two requirements: (1) incompatibility of A and B involving a restricted volume effect (A and B chains being confined in A and B domains, respectively) and (2) incompressibility of polymeric solids involving uniform filling of A and B domains by A and B segments, respectively.

In section IV, we shall review some experimental results on microdomain structure in solid state, long-range spatial order of the domains, domain-sizes as a function of molecular weights, orientation of the lamellar or cylindrical domains, and equilibrium and non-equilibrium aspects of the domain morphology. The experimental results will be analyzed in the light of the theories which will be discussed in section III to investigate the molecular conformation and molecular packing in the microdomains, and the relationship between the domain size and the molecular dimension.

Finally in section V we shall review very recent results on SAXS (small-angle X-ray scattering) analyses of the polymer-polymer interphase in block polymers. The experimental results will be compared with the equilibrium theories discussed in section III.

II. Microphase Separation in Solution

II-1. Structure of Block Polymers in Concentrated Solutions

The existence of the ordered structure in polystyrene-polybutadiene diblock polymer solution was suggested by Vanzo in 1966[1]. It was he who observed the reflectance of visible light from the solution as a function of wavelength (Figure 1(a)) and showed that maximum reflectance increased abruptly at around 9 % for this particular polymer-solvent system (Figure 1(b)). The abrupt change of the reflectance with concentration may reflect a critical concentration above which an ordered structure is formed in the solution. Moreover, the identity period of this ordered structure is shown to increase with an increasing polymer concentration, as shown in Figure 1(a).

Further quantitative and systematic studies on the structure of the concentrated block polymer solutions have been carried out extensively by French groups, Sadron, Gallot and Skoulios[2,3] and also by Hoffmann and his co-workers[4] in Germany.

Figure 2 shows an isotherm phase diagram drawn by Sadron and Gallot[2] for

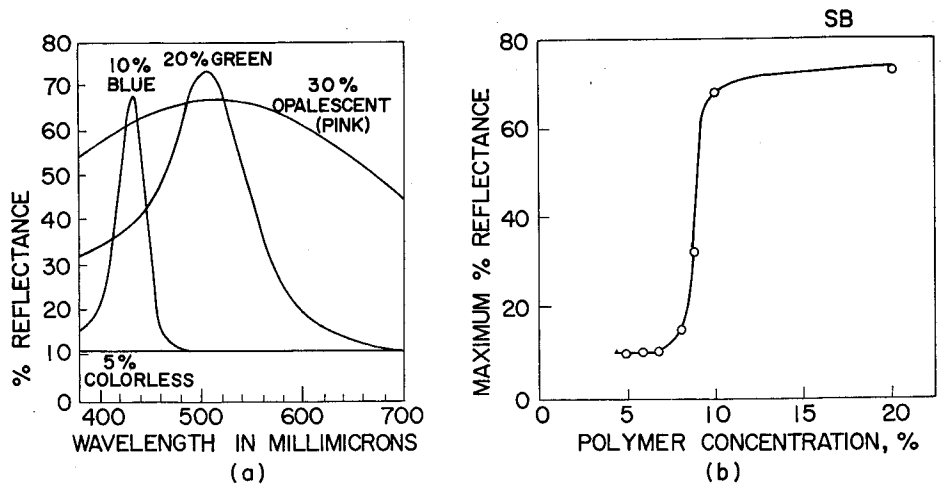

Fig. 1. (a) The spectral distribution of reflectance of visible light for polystyrene-polybutadiene diblock polymer solutions (5, 10, 20 and 30% ethylbenzene solutions) and (b) the maximum reflectance as a function of polymer concentrations (Vanzo, 1966).

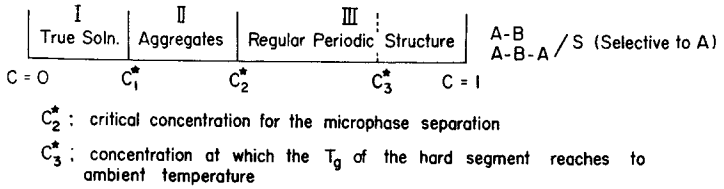

Fig. 2. An isotherm phase diagram for A-B diblock and A-B-A triblock polymers in the solvents selectively good for A polymers. The concentration C_3^* is added by the present authors. (Sadron and Gallot, 1973).

A-B diblock and A-B-A triblock polymers in the solvents selectively good for A polymers. In region I where the concentration is very low the polymers are molecularly dispersed and a true solution is obtained. At higher concentrations, molecules tend to aggregate to form intermolecular micelles, and C_1^* is the critical concentration for the aggregate formation. However, the aggregates themselves do not form the long-range order or regular periodic structure in solution at this concentration range.

At still higher concentrations is formed a regular periodic structure in solution. We shall define this concentration C_2^* as a critical concentration for the microphase separation. It is believed to be this concentration C_2^* which gives rise to an abrupt increase of the maximum reflectance, as observed by Vanzo.

We added an additional critical concentration C_3^* to the phase diagram, i.e., the concentration above which the systems cannot attain, or have difficulties to attain, equilibrium. The glass transition temperature (T_g) of the A and B block

segments increases with concentration. When the T_g of the hard segment (i.e., the segment having a higher T_g) reaches an ambient temperature with increasing concentration, the system cannot attain a new equilibrium with a further increase of the concentration, since the microbrownian motion of the hard segment is frozen. We shall discuss this non-equilibrium effect in section IV-4.

Sadron and his co-workers studied the structure in concentrated solutions by using a unique technique of the post-polymerization of the solvent. Namely, they used, as the preferential solvent, the monomers which can be easily polymerized by irradiation with U.V. light. Figure 3 shows a typical solidified structure in

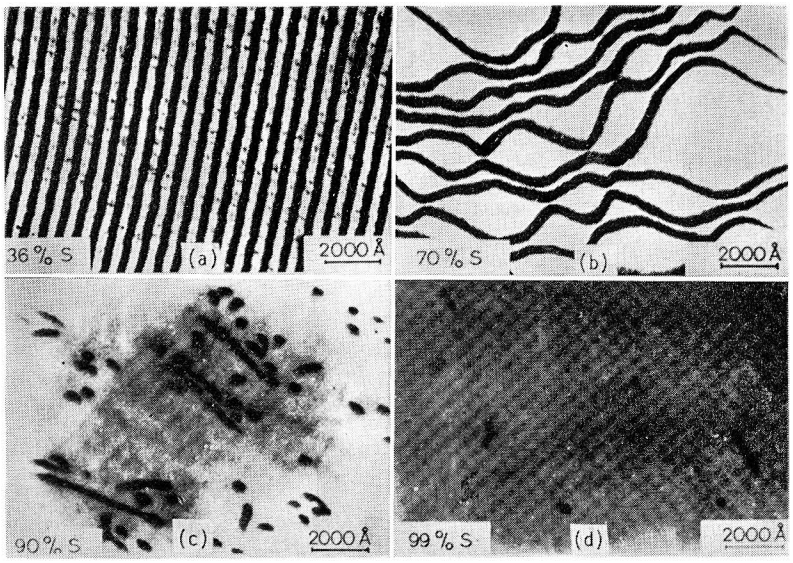

Fig. 3. Typical solidified structures in the solutions of polystyrene-polybutadiene diblock polymer in styrene as a solvent; (a) 36%, (b) 70%, (c) 90%, and (d) 99% solvent content. (Sadron and Gallot, 1973).

solutions of polystyrene-polybutadiene (S-B) diblock polymer in styrene. Styrene is a solvent selectively good for polystyrene (PS). The structure in the solution was solidified by polymerizing the solvent, and then being selectively stained by osmium tetroxide for observation under transmission electron microscopy. (The dark and white regions in the micrographs correspond, respectively, to the stained polybutadiene (PB) and unstained PS phase composed of PS block chains and polymerized styrene monomers.) The results shown in Figure 3 indicate a structural change encountered by a dilution of the system from region III to II in Figure 2. The long-range order is destroyed (Figure 3(a) to 3(b)), and the aggregates change their size and shape with a decrease of the polymer concentration (Figure 3(c) to 3(d)).

Change of the domain structure with concentration in region III in Figure 2 has been again studied extensively by Sadron and Gallot et al[2]. and by Skoulios et al.[3]. Sadron and Gallot showed that there are two kinds of system: (a) one in which only one type of domain structure (either spherical, cylindrical or lamellar morphology) can be observed with varying concentration in Region III, and (b) the other in which morphological transitions from sphere to cylinder, or from cylinder to lamella take place by increasing the concentration as illustrated in Figure 4. The diblock polymers such as S-B, polystyrene-polyisoprene (S-I),

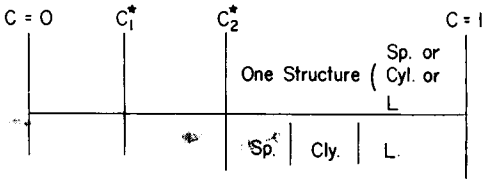

a) PS/PB, PS/PI, PI/PVP, PI/PMMA

b) PS/P2VP, PS/P4VP, PMMA/PHMA

Fig. 4. Order structures in the concentration regime III in Figure 3 and the change of the structures with concentration as may be summarized from the works of Sadron and Gallot.

polyisoprene-polyvinylpyridine (PS/PVP), and polyisoprene-polymethylmethacrylate (PI/PMMA) belong to the former group. Polystyrene-poly-2-vinylpyridine (PS/PVP), polystyrene-poly-4-vinylpyridine (PS/P4VP) and polymethylmethacrylate-polyhexylmethacrylate (PMMA/PHMA) belong to the latter group. However, the physical factors by which the two groups are classified were not discussed by the authors, and still remain to be solved at the present stage.

Figure 5 illustrates typical solidified structures and schematic diagrams showing molecular packing in the domain structures of S-B diblock polymers in methylmethacrylate which is a selectively good solvent for PS block chains and is post-polymerized by U.V. irradiation. All three structures shown in Figures 5(a) to 5(c) are at 30 % solvent content. The alternating lamellar structure of Figure 5(a) corresponds to the case where the molecular volumes of PS and PB in the solution are about equal. On the other hand, the cylindrical structure shown in Figures 5(b) (or 5(c)) corresponds to the case where the molecular volume of PS (or PB) is smaller than the other.

Figures 6(a) and 6(b) show, respectively, typical changes of the structure parameters of the domains corresponding to Figure 5(a) and 5(c) with the solvent

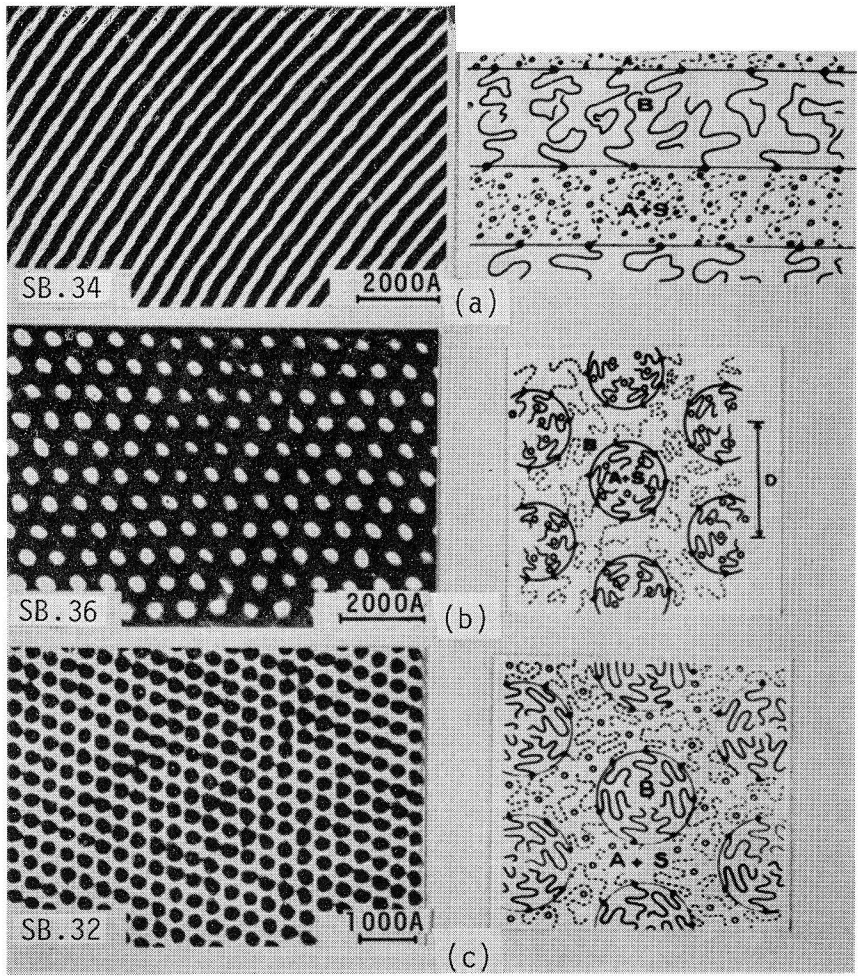

Fig. 5. Typical solidified structures for polystyrene-polybutadiene diblock polymers in methylmethacrylate in the concentration regime III and schematic diagrams showing arrangement of the molecules in the respective domain structure, (a) alternating lamellar, (b) swollen polystyrene rods in polybutadiene matrix, and (c) polybutadiene rods in swollen polystyrene matrix. The symbols A, B and S stand for polystyrene, polybutadiene, and methylmethacrylate. (Sadron and Gallot, 1973).

content. It should be noted that these systems are those in which only one type of domain structure is observed with varying concentration. The parameters estimated by the small-angle X-ray scattering (SAXS) technique are (1) the thicknesses of A and B lamellar domains, d_A and d_B, in Figure 5(a), (2) the domain identity period $D=d_A+d_B$, (3) the interfacial area occupied by a single chain S, (4) the radius of the cylindrical domain R and (5) the inter-cylinder distance D. In the case of the lamellar domain, the distance between the neighbouring chemical junction

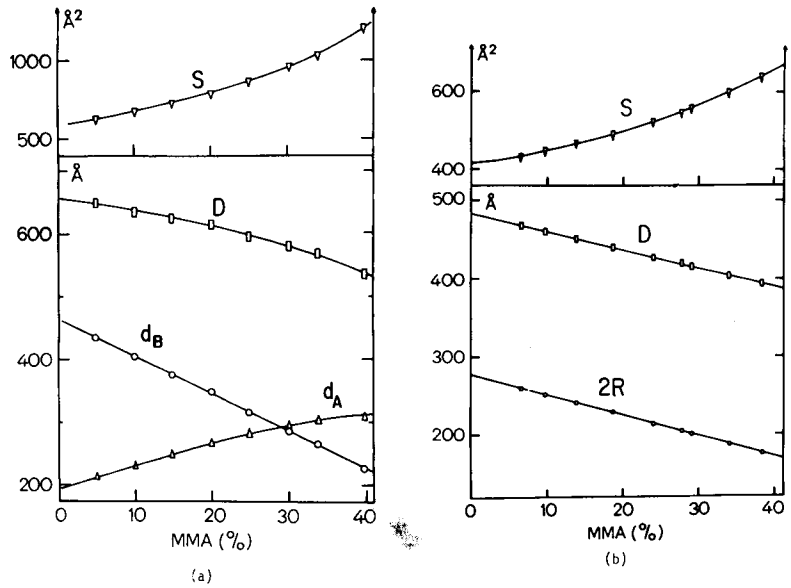

Fig. 6. Variations of (a) the lamellar thicknesses d_A and d_B (for polystyrene and polybutadiene lamellae, respectively) and the domain identity period $D=d_A+d_B$ and the interfacial area occupied by a block chain S for the lamellar domain system shown in Figure 5(a), and (b) variations of the radius of the polybutadiene rods R, the inter-rod distance D and the interfacial area S for the cylindrical domain system shown in Figure 5(c) as a function of the solvent content. (Sadron and Gallot, 1973).

points or the interfacial area S increases with an increasing amount of solvent due to a swelling in lateral directions, which results in decreasing the sizes d_B and D, as shown in Figure 6(a). However, the solvent which selectively swells the PS-domain tends to expand the thickness d_A. This expansion outweighs the contraction due to the swelling in the lateral direction, resulting in an increase of thickness of PS lamellae with increasing solvent content. The same argument can be applied to the cylindrical system.

A consequence of the microphase separation on the rheological behavior of the block copolymer solution has recently been studied by Pico and Williams[5]. Figure 7 shows a dramatic change in rheological behavior with increasing solvent content at a given temperature 75°C. As shown in the figure, the shear-rate dependence of the real part of the dynamic viscosity shows a transition from non-Newtonian to Newtonian behaviors with increasing solvent fraction for the PS-PB-PS triblock polymer (S-B-S) in dipentene. (The corresponding block molecular weights are 9.6, 47.5 and 9.4×10^3, respectively.) For a given polymer-solvent system, the critical concentration is a function of temperature or the critical temperature is a function of concentration. The critical temperature is shown to

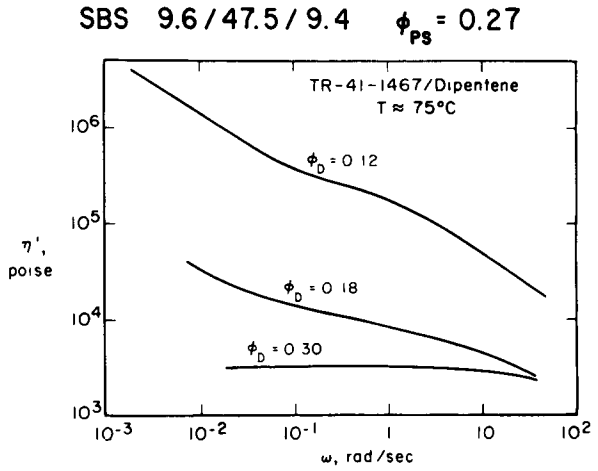

Fig. 7. Frequency dependence of real part of dynamic viscosity for polystyrene-polybutadiene-polystyrene triblock polymers in dipentene at 75°C. ϕ_D designates the volume fraction of the solvent. (Pico and Williams, 1977).

Table 1. T_c Transition Temperature for TR-41-1467-Dipentene (Pico and Williams, 1977)

Percent solvent	Optical range, °C	Rheological range, °C
12	99–112	95–112
18	77–93	76–92
30	63–77	50–76

correlate closely to the temperature at which the transmission of visible light changes, as shown in Table I. Thus, the critical concentration as observed by the rheological measurements may reflect the critical concentration C_2^* for the microphase separation. The critical temperature is considered to reflect the temperature at which the microphase-separated structure is melted into a homogeneous mixture or its reverse transition. It is natural that the critical temperature decreases with increasing solvent content.

II-2 A New and Novel Technique

It is essential, from both scientific and technological view points, to understand the critical temperature or concentration in terms of the molecular parameters of block polymers such as (i) total molecular weight, (ii) composition, (iii) energetic interactions among A and B block chains and solvents and (iv) molecular architecture. Since the structure formed at the critical concentration or the critical temperature is some few ten nanometers, the small-angle X-ray scattering (SAXS) technique will be the most suitable technique to characterize the domain structure

in the solution, or the transition phenomena such as the phase-separation, or the homogenization.

A remarkable advance of the SAXS technique has recently been achieved with an advance of techniques in position sensitive X-ray detectors and high flux X-ray sources. The new SAXS technique enables one to measure the scattering profiles with much less exposure time to X-ray. Consequently, it enables one to study the kinetics of structural formation occurring during the crystallization[6] or phase transition in multicomponent systems.[7]

Figure 8 shows a schematic diagram of our rapid X-ray detecting system for

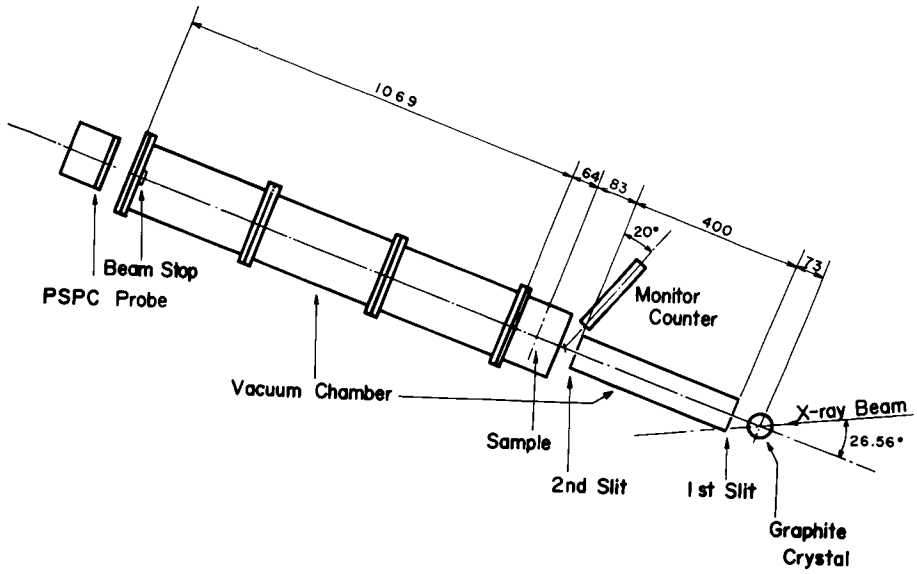

Fig. 8. A schematic diagram of the dynamic small-angle X-ray scattering apparatus with a rotating anode X-ray generator of 12 kW and a multi-wired delay line type position sensitive proportional counter. (Hashimoto et al., 1980).

SAXS, which utilizes a rotating anode X-ray generator of 12 kW and a multi-wired delay line type position sensitive proportional counter (PSPC). The incident beam is monochromatized into CuKα-radiation by a graphite crystal and a pulse-height analyzer. The detailed descriptions of the apparatus will be given eleswhere[8].

Figure 9 shows the preliminary results on the change of the SAXS curve upon heating (a) and cooling (b) 56 wt % toluene solutions of S-I diblock polymer having a total molecular weight of 31×10^3 and 40 wt % PS. Each scattering curve was obtained with 100 sec. exposure to the X-ray beam, and one channel corresponds to one minute in the scattering angle. The origin of each curve is shifted in a diagonal direction to avoid an overlapping of the curves. The scatter-

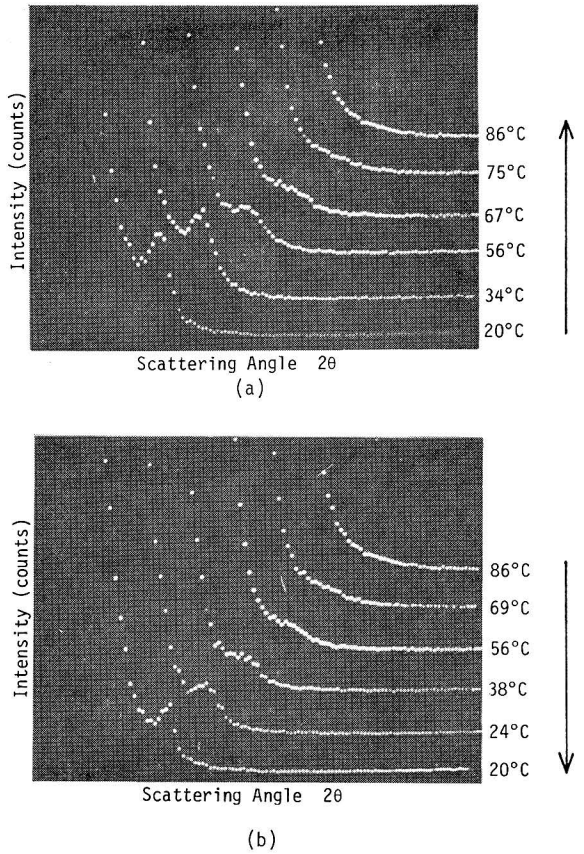

Fig. 9. Oscilloscope traces showing variations of the SAXS curves with (a) heating and (b) cooling 56 wt % toluene solutions of polystyrene-polyisoprene diblock polymer (specimen L-2 in the text). Each curve was obtained for 100 sec. exposure to X-ray beam and one channel corresponds to one minute in scattering angle. Origin of each curve is shifted in diagonal direction to avoid an overlap of the curves. CuKα-radiation.

ing maximum is shown to disappear at about 86°C with increasing temperature, and appears reversibly with decreasing temperature.

More quantitative aspects of these results are shown in Figure 10, where the results of Figure 9 on the heating cycle are replotted. The three important effects observed with increasing temperature are: (i) the peak-height decreases (ii) the peak-position shifts toward larger scattering angles, and (iii) the peak-breadth increases. They all suggest a melting of the phase-separated structure in solution into a homogeneous mixture with an increasing temperature. With an increasing temperature, the interfacial tension decreases and thus the incompatible block chains

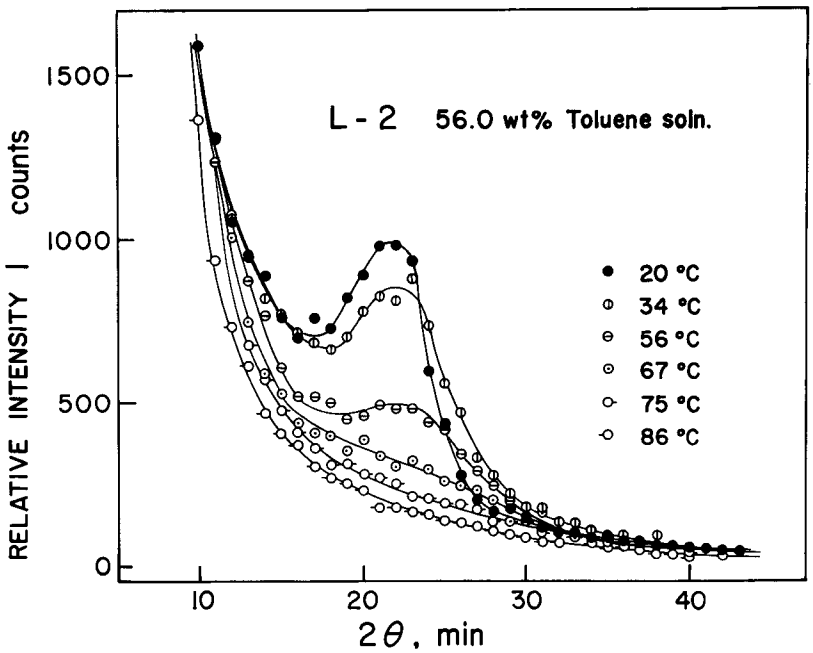

Fig. 10. Replot of the results in Figure 9 for the heating cycle. The change of the curves with temperatures suggests a melting of the phase separated structure in solution into a homogeneous mixture with increasing temperature.

tend to mix, which results in decreasing the long identity period of the domain structure.

Figure 11 shows a schematic diagram of five fundamental microdomain structures of block copolymers in solid state. It shows that the domain morphology, varies from A spheres and A cylinders in B-matrix, alternating A and B lamellae,

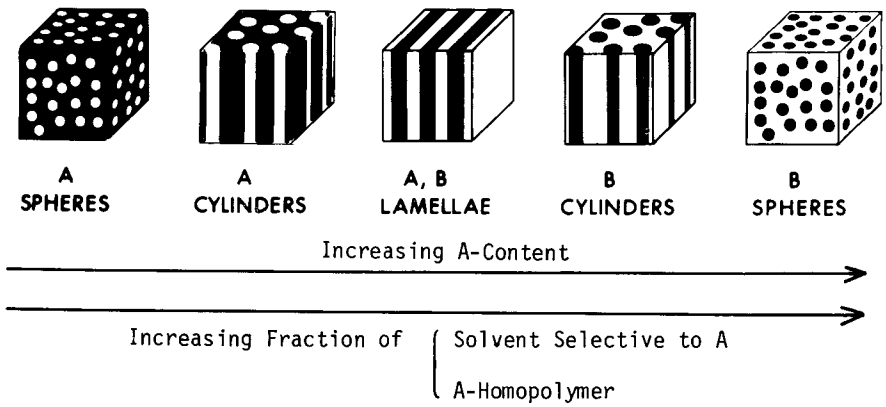

Fig. 11. Five fundamental microdomain structures of block polymers in bulk, block polymer-(solubilized) homopolymer systems, and block polymers in solutions.

B cylinders and B spheres in A, with an increasing molecular volume of A block chain relative to that of B. It can be shown that this diagram, originally proposed by Molau[9] for solid state morphology of pure block polymers, may be extended to the domain structure in the solutions at concentrations higher than the critical concentration C_2^* for the microphase separation. In this case, one should consider the molecular volumes of A and B in solutions instead of those in bulk. Thus, with an increasing fraction of a solvent selective to A, the molecular volume of A block chains and volume fraction of A domains increase relative to that of B block chains and of B domains. This provides a driving force toward the morphological transitions from A spheres to A cylinders, A cylinders to the alternating lamellae etc. This kind of morphological transition has been shown to occur by adding A-homopolymers as far as A-homopolymers can be solubilized into A-domains[10]. However it should be noted that the long-range order of the domains tends to be destroyed with an increasing fraction of solvent, or solubilized homopolymers, in contrast to the morphological transition induced by changing the chemical composition of the block polymers.

III. Microphase Separation in Bulk

For block polymers such as S-I which have an upper critical solution temperature, the microphase separation occurs by lowering the temperature below the critical temperature T_c. In this section, we shall briefly review equilibrium theories of the microphase separation in bulk, and also some effects of the microphase separation on bulk properties.

III-1. Theoretical Aspects

Let us first consider some fundamental physical factors which control morphology of the microdomain structure in equilibrium state. Deep insights into the physics underlying the microphase separation were first given by Meier[11], and later by Helfand[14]. The interaction between A and B segments is repulsive, and therefore gives a driving force toward growth of the domains so as to reduce the surface-to-volume ratio. When the domain grows it tends to create a density difficiency toward the center of the domain. Since the polymeric solid is highly incompressible, it is energetically unfavorable to create a density difficiency. Thus, only those conformations of block polymer chains which fill the space in the center of the domain are allowed to satisfy the demand of the uniform space-filling. This involves the loss of conformational entropy, and this entropy loss which increases with increasing the domain size acts as an opposing force toward the domain-growth. The loss of entropy to confine the junction points somewhere

in the interphase also increases as the domain grows, because the volume fraction of the interphase decreases as the domain grows. This factor also opposes the domain growth. Therefore, the equilibrium morphology of the domains such as size, shape and spatial arrangement of the domains and the interfacial structure should be determined by a balance of these three factors. These factors, in turn, are a function of molecular properties of the block polymers, i.e., molecular weight, chemical composition, the interaction parameter and molecular architecture.

Many theories[11-21] have been proposed to describe such equilibrium aspects of domain morphology. However, the theories proposed by Meier[11-13] and by Helfand et al.[14-16] seem to be most elaborate and to be capable of describing the experimental results most quantitatively. They treated the theories as statistical mechanics of random-flight chains in the confined "domain space" subjected to the requirement of the uniform space-filling.

For example, free energy change ΔG forming the lamellar microdomains from a uniform mixture, in the context of the narrow interphase approximation of Helfand and Wasserman[15], is given by:

$$\begin{aligned}\frac{\Delta G}{Nk_BT} = {} & \frac{2\gamma}{k_BT}\left(\frac{Z_A}{\rho_{0A}}+\frac{Z_B}{\rho_{0B}}\right)\frac{1}{D}-\ln\frac{2a_I}{D} \\ & +0.141\,\frac{(Z_A^{1/2}/b_A\rho_{0A})^{2.5}+(Z_B^{1/2}/b_B\rho_{0B})^{2.5}}{[(Z_A/\rho_{0A})+(Z_B/\rho_{0B})]^{2.5}}D^{2.5} \\ & -\alpha\frac{(Z_A/\rho_{0A})(Z_B/\rho_{0B})}{(Z_A/\rho_{0A})+(Z_B/\rho_{0B})}\end{aligned} \tag{1}$$

where γ is the interfacial tension given by

$$\gamma = k_BT\alpha^{1/2}\left[\frac{\beta_A+\beta_B}{2}+\frac{1}{6}\frac{(\beta_A-\beta_B)^2}{\beta_A+\beta_B}\right] \tag{2}$$

a_I is the interfacial thickness given by

$$a_I \equiv 1/(d\tilde{\rho}_A/dZ)_{\tilde{\rho}_A=1/2} = 2\left(\frac{\beta_A^2+\beta_B^2}{2\alpha}\right)^{1/2} \tag{3}$$

and

$$\beta_k = \rho_{0k}b_k^2/6\,, \quad b_k^2 = \langle R_k^2\rangle_0/Z_k \tag{4}$$

where b_k is Kuhn's statistical segment length, Z_k is the degree of polymerization of the k block chain, ρ_{0k} is the number density of the segment in pure polymer, $\tilde{\rho}_k$ is defined as $\rho_k(\boldsymbol{r})/\rho_{0k}$ where $\rho_k(\boldsymbol{r})$ is the local segment density in the interphase, and D is the domain identity period, i.e., the sum of the A and B lamellar thicknesses. The parameter α is the interaction parameter as defined by

$$\alpha = (\delta_A - \delta_B)^2 / k_B T \qquad (5)$$

where δ_k is the solubility parameter of the k-chain and k_B is the Boltzmann constant. The quantity N is the number of block polymer chains incorporated in the microdomain formation.

The first term on the right hand side of eq. (1) is associated with the interfacial free energy, which is composed of the interaction energy of mixing A and B segments and the loss of conformational entropy to maintain uniform density in the interphase. The interfacial energy is proportional to 1/D. The second term is the loss of the placement entropy which increases ΔG in proportion to ln D. The third term is associated with the loss of conformational entropy due to the constraint volume effect (i.e., the effect of A and B chains being restricted in A and B domains, respectively) and to the uniform space-filling. This term contributes to ΔG in proportion to $D^{2.5}$. The last term is the enthalpy of demixing. The combinatorial entropy term is trivial and ignored in this treatment.

Eq. (1) neglects the non-locality of energetic interaction. If this non-locality should be taken into account, γ in eq. (1) should be replaced by eq. (6.7) of Helfand and Sapse (HS)[22], and a_I in eq. (3) should be calculated from eq. (6.5) of HS, the results of which turn out to be explicitly given by[23]

$$a_{I,nl} = 2\left[\frac{\beta_A^2 + \beta_B^2}{2\alpha} + \frac{1}{6}\sigma_I^2\right]^{1/2} \qquad (6)$$

where σ_I is the interaction range parameter of monomer units ($\sim$0.5 nm). The equilibrium value of D is given by minimizing ΔG with respect to D.

A similar equation for ΔG has been derived by Meier[11-13] which will be described elsewhere[23].

III-2. Critical Temperature

The critical temperature T_c, at which the microphase-separated structure melts into a homogeneous mixture, is obtained from the condition

$$\Delta G(T = T_c) = 0 \qquad (7)$$

Figure 12 shows the critical temperature T_c calculated from eq. (1) for the S–I diblock polymer having a lamellar morphology[15] (50 wt % PS), or from the theory for the same diblock polymer having a spherical domain morphology[16] (20 wt % PS or PI block). The molecular parameters used for the calculation will be described in detail in section IV-3.

It is obvious from the figure that the temperature T_c strongly depends on the molecular weight and chemical composition of the block polymer. T_c also de-

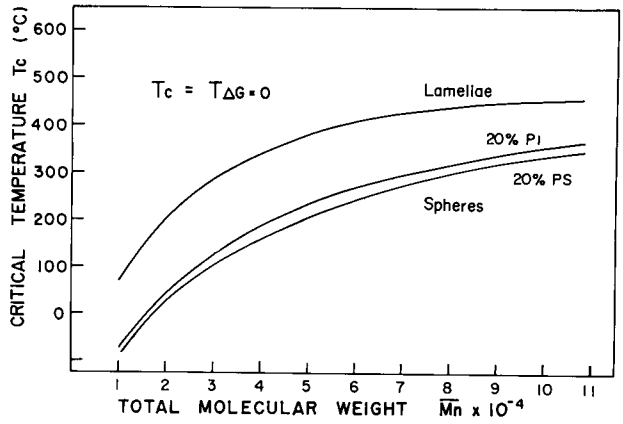

Fig. 12. Critical temperature T_c calculated from the theoreies of Helfand and Wasserman for polystyrene-polyisoprene diblock polymers having lamellar morphology (50 wt % polystyrene) and for the same diblock polymers having the spherical domain morphology (20 wt % polystyrene or polyisoprene).

pends on the interaction parameter α, the greater the value of α the higher the T_c. The minor difference in T_c for the two spherical domains is due to an asymmetric effect, i.e., the densities, the statistical segment length and the degree of polymerization being different for the two cases. Thus, for the block polymers composed of the block chains having large molecular weights and a high repulsive interaction α, the microphase-separated structure may not necessarily be melted into the homogeneous mixture, or may not be formed from the homogeneous mixture without thermal degradation.

Figure 13 shows a typical change of the SAXS profiles with temperature during (a) heating and (b) cooling the specimens[7]. Each curve was obtained with the PSPC detector with 40 sec. exposure to X-ray, and one channel corresponds to one minute in the scattering angle. The specimen is styrene-isoprene "tapered" block copolymer, having a total number-average molecular weight of 4.3×10^4 and weight fraction of styrene 0.47. In the tapered polymer there is a mixing of styrene and isoprene monomers in the primary structure, which apparently decreases the interfacial tension between "polystyrene-rich" block segments and "polyisoprene-rich" block segments. Consequently it enhances a mixing between them, resulting in decreasing T_c. It is seen that the scattering maximum corresponding to a long identity period of the phase-separated domains disappears with an elevating temperature at around 170°C, and appears again in the same scattering angle with decreasing temperature. This temperature 170°C is related to T_c and much lower than the temperature for ideal block polymers

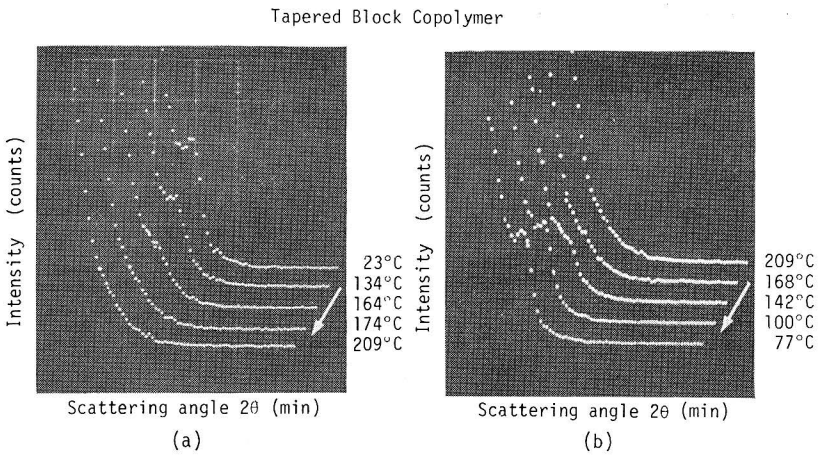

Fig. 13. Variation of the SAXS curves with temperature during (a) heating and (b) cooling the tapered styrene-isoprene block copolymers in bulk (the specimens having a total molecular weight 4.3×10^4 and weight fraction of styrene 47 %). Each curve was obtained with the PSPC-SAXS apparatus with 40 sec. exposure to X-ray and one channel corresponds to one minute in scattering angle (Cukα-radiation). (Hashimoto, Tsukahara, and Kawai, 1980).

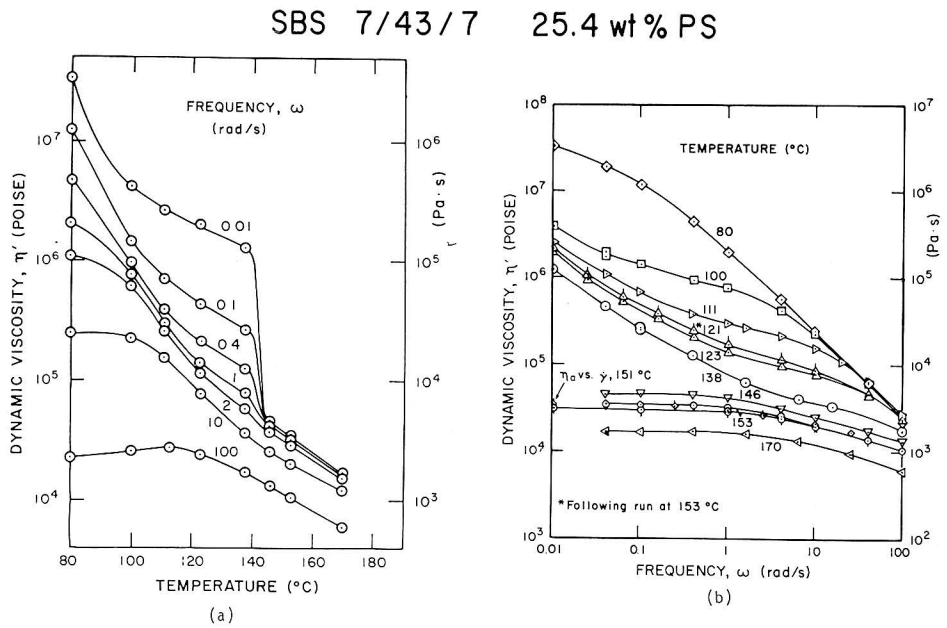

Fig. 14. Real part of dynamic viscosity (a) as a function of temperature at various frequencies and (b) as a function of frequency at various temperatures for polystyrene-polybutadiene-polystyrene triblock polymers in bulk. (Gouinlock and Porter, 1977).

having corresponding block molecular weights[24].

Figure 14 shows a consequence of the microphase separation, or its reverse transition on the rheological behavior of S-B-S triblock polymers having corresponding block molecular weights of 7-43-7 in units of thousands, respectively[25]. The isotherms of the real part of dynamic viscosity show a transition from non-Newtonian to Newtonian at about 140°C (Figure 14(b)). The isochronal data in Figure 14(a) also show this transition which is believed to be closely related to the transition of microphase-separation. The transition temperature is shown to agree with that expected from Helfand's theory[16].

IV. Microdomain Structure in Solid State

IV-1. Long-Range Order

Figure 15 shows a typical microdomain structure in solid state observed for S-I diblock polymers; (a) spherical and (b) cylindrical polyisoprene domains dispersed in polystyrene matrix, and (c) alternating lamellar domains. There are phase-inverted domain structures for spherical and cylindrical morphologies which are not shown in the figure. The left and right half of (b) are the sections occasionally cut nearly normal and parallel to the cylindrical domains, respectively. The figure indicates that the spherical, cylindrical and lamellar domains are regularly arranged in space, possesing a long-range order attributable to the entropic repulsion between the dispersed domains.

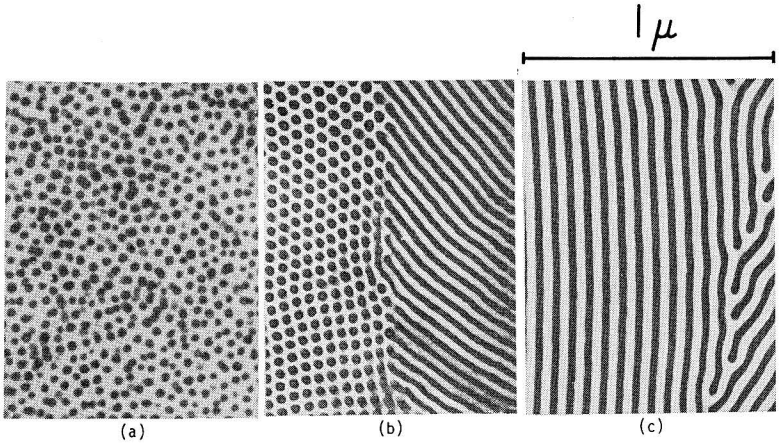

Fig. 15. Typical microdomain structure in solid state prepared by solvent casting of toluene solutions of polystyrene-polyisoprene diblock polymers; (a) spherical and (b) cylindrical polysioprene domains dispersed in polystyrene matrix, and (c) alternating lamellar domains. The corresponding molecular weights of polystyrene and polyisoprene blocks are 251/71, 582/313, and 62/44 in units of thousands for the figures (a), (b), and (c), respectively.

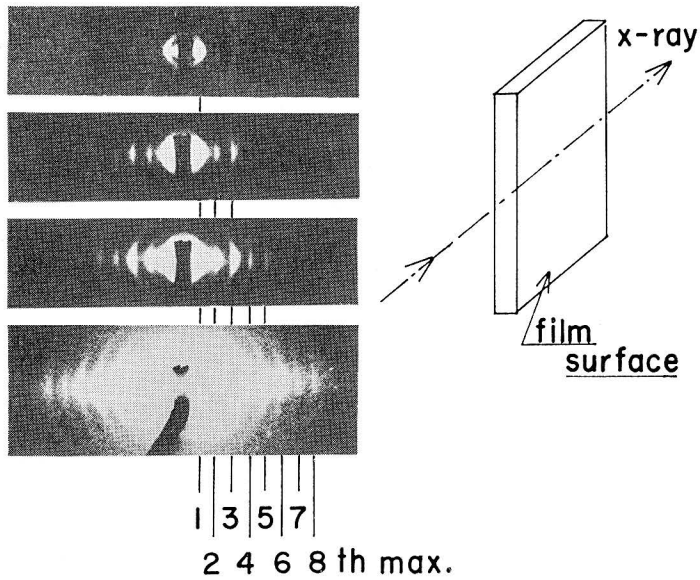

Fig. 16. Typical SAXS patterns from a specimen having the lamellar microdomains taken with incident X-ray beam parallel to the film surfaces. The patterns were taken with 4 different exposures to show a number of scattering maxima with a Huxley-Holmes camera and a high-brilliancy rotating anode X-ray generator. (Hashimoto, Todo, Itoi and Kawai, 1977).

Figure 16 shows typical SAXS patterns from a specimen having the lamellar microdomains taken with an incident X-ray beam parallel to the film surfaces as shown in the figure[26]. The patterns were taken with four different exposures to show a number of scattering maxima. They were taken with a Huxley-Holmes camera and a high-brilliancy rotating anode X-ray generator as a fine focussed X-ray source (40 kV$\times$30 mA, effective focal spot area 0.1×0.1 mm^2). The intensity profiles in the equatorial direction of the patterns, i.e., in a direction parallel to the film, normals were more quantitatively measured by a scintillation cournter for a series of block polymers having a lamellar morphology with a different long-identity period D. (See Table II.) The results are shown in Figure 17, in which each curve shows a number of higher-order scattering maxima arising from a single lamellar spacing D[23]. The spacing, calculated from each maximum based on Bragg's equation, agrees with an error of less than about 1 %.

A paracrystalline analysis of these scattering curves show that the relative peak heights are related to the volume fraction of A and B domains, and that the number of resolvable scattering maximum is related to the uniformity of the domain size[27]. For example, the SAXS profile for L-6 exhibits at least up to the 9-th order maximum, indicating that the standard deviation for the fluctuation

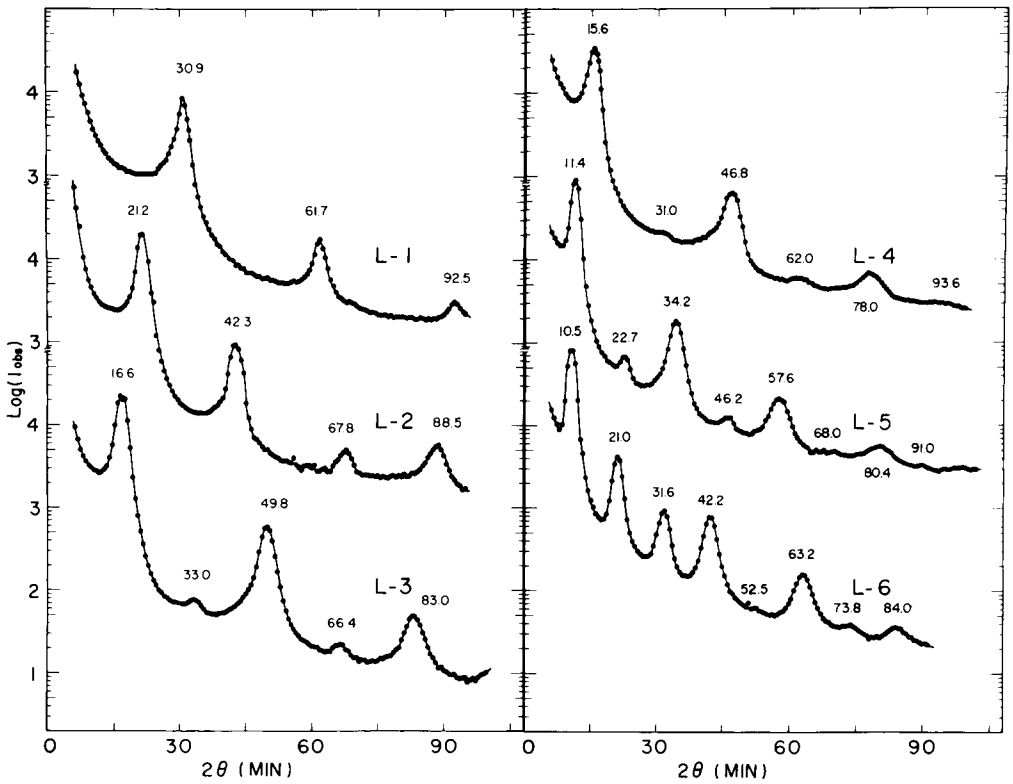

Fig. 17. The SAXS intensity profiles for a series of block polymers having lamellar morphology in the direction parallel to film normal, i.e., in the equatorial direction of Figure 16. (Hashimoto, Shibayama, and Kawai, 1980).

in the lamellar spacing is about 4 %[23,27].

Such a long-range order in the spatial arrangements of the domain structure has also been observed by many workers, notably by Keller and co-workers[28,29] for the lamellar and cylindrical domains, Hoffmann and co-workers[4,30] for the cylindrical domains, and Hashimoto and co-workers[31] for the spherical domains.

In Figure 18, the curve drawn with open circles shows a typical measured scattering function for specimen SI-4 (See Table III for the characterization) having a spherical domain system[31]. The scattering curve was corrected for absorption, air-scattering, slit-length and slit-width smearing effects, and the background scattering arising form the local atomic order within each phase. We can conclude that the first four peaks or shoulders (marked by diamond-shaped marks) are those arising from inter-particle interference, their relative angular positions being $1:\sqrt{2}:\sqrt{3}:\sqrt{4}$, indicating that the spherical domains have such a regular spatial arrangement as simple cubic lattice or cubic-closed parking

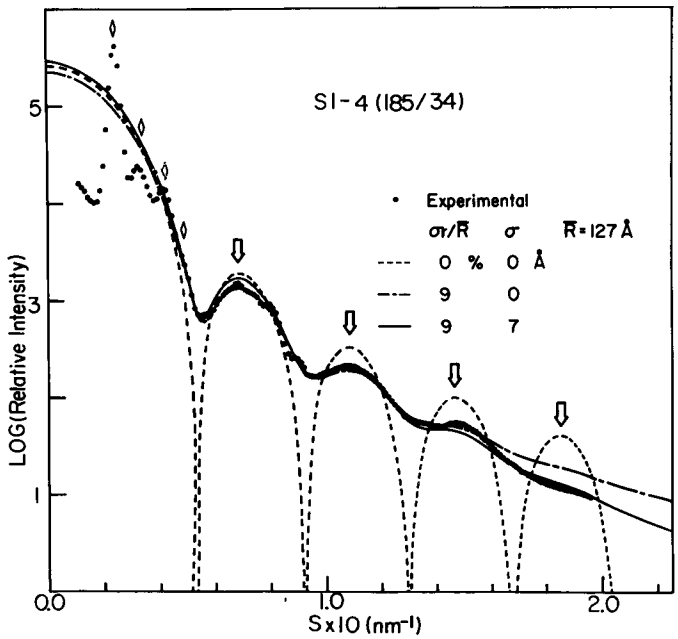

Fig. 18. A typical measured scattering function for a specimen SI-4 in Table III having spherical domain morphology (open circles) and the calculated scattering curves for isolated spheres; sphere having monodisperse size and sharp boundary (broken line), sphere having a Gaussian size distribution and sharp boundary (dash-dot line), and sphere having the Gaussian size distribution and diffuse boundary (solid line). The measured curve was corrected for absorption, air scattering, slit-length and slit-width smearing effects, and the background scattering arising from the local atomic order within each phase. (Hashimoto, Fujimura, and Kawai, 1980).

(somewhat distorted so that the extinction rule for the perfect crystal may not be applied). In any case, the number of the inter-particle interference maxima demonstrates the existence of the long-range order in spherical domain systems.

The origin of such long-range regularity of spherical domains can be interpreted again in terms of the entropic repulsion between the spheres, which can be quantitatively predicted in the context of the confined chain-statistics. The four broad maxima marked by arrows are attributed to the first to fourth-order intra-particle interference maxima observed for an isolated sphere. If the sphere is fairly monodisperse, its size can be estimated from the peak position of i-th maximum, i.e.,

$$U_{\max,i} = 4\pi(R/\lambda)\sin\theta_{\max,i} = 5.765, 9.10, 12.3, \cdots \quad \text{for } i = 1, 2, 3, \cdots \tag{8}$$

The curve drawn by the broken line corresponds to the calculated curve from

an isolated sphere of radius 12.7 nm. The curve drawn by a dash-dot line corresponds to the curve from an isolated sphere having a Gaussian type size distribution, $\bar{R}=12.7$ nm and $\sigma_r/\bar{R}=0.09$.

$$P(R) = (2\pi\sigma_r^2)^{-1/2} \exp\left[-(R-\bar{R})^2/2\sigma_r^2\right] \quad (9)$$

It is clearly seen that the calculated result fits better with the experimental result by introducing the size distribution. However, the calculated curve still deviates from the measured curve, in that the measured curve drops more rapidly than the calculated one with the scattering angle. This deviation may be attributed to the effect of the diffuse-boundary, as will be discussed in section V. In fact, the agreement becomes almost perfect by introducing the diffuse boundary, as characterized by the parameter $\sigma=0.7$ nm. Table III summarizes the size distribution of the spherical domains. The size of the domain itself is seen to be fairly monodisperse.

Similarly, the SAXS patterns for the block polymers having cylindrical domains usually show a number of scattering maxima, indicating the existence of the long-range order of the domain and fairly monodispersed domains. Figure 19 shows a typical SAXS pattern for the rodlike domain (S-I diblock having

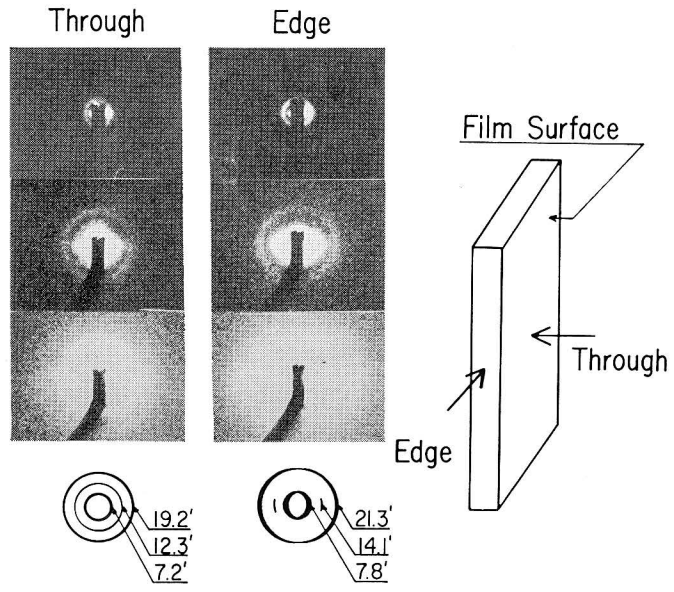

Fig. 19. Typical SAXS patterns for polystyrene-polyisoprene diblock polymers having the cylindrical domain of polyisoprene dispersed in the matrix of polystyrene; (a) through-view and (b) edge-view with 3 different exposure times. The block molecular weights of polystyrene and polyisoprene are 150 and 74 in units of thousands.

molecular weights of PS and PI sequences, 74 and 150×10^3 g/mol, respectively).

IV-2. Orientation

Figures 16 and 19 clearly show that the lamellar and cylindrical domains in the solvent-cast films have preferred orientation. Namely, in case of the lamellar morphology, the scattering appears perpendicular to the film surfaces, indicating that the lamellar domains are highly oriented with their boundaries parallel to the film surfaces (see Figure 20). The SAXS pattern taken with an incident X-ray beam normal to the film surfaces is circularly symmetric, indicating that the orientation of the lamellar normal is uniaxially symmetric with respect to the film normal.

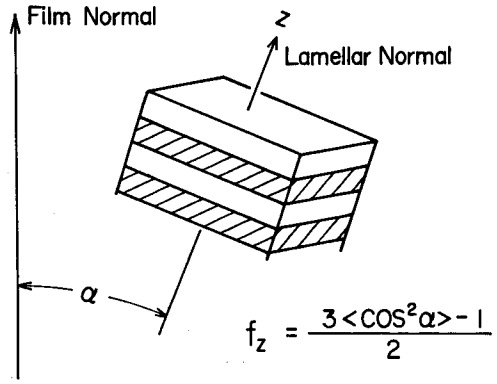

Fig. 20. The orientation factor of the lamellar normal with respect to the film normal (Hashimoto, Shibayama, and Kawai, 1980).

The degree of lamellar orientation was estimated by measuring the integrated intensity as a function of the azimuthal angle[26]. The analyses indicated that the second-order orientation factor $f_z=[3\langle\cos^2\alpha\rangle-1]/2$ is 0.95, indicating an almost perfect orientation of the lamellar domains[23].

In the case of cylindrical domains, the axes of cylinders are usually shown to be preferentially oriented parallel to the film surfaces as will be obvious from Figure 19.

Such a high degree of domain orientation has been observed also by Keller and co-workers for the extruded SBS materials[28,29]. In this case also the domain interfaces are oriented parallel to the surface of the extruded materials.

IV-3. Domain Size, Molecular Dimension, and Molecular Packing in Lamellar Microdomains

Table II shows a summary of the results obtained for a series of S-I diblock

Table 2. Measured Domain-Properties of Polystyrene-Polyisoprene Diblock Copolymers Having Lamellar Morphology
(Hashimoto, Shibayama, and Kawai, 1980)

Specimen Code	Total $\bar{M}n \times 10^{-3}$	wt% PS	Domain Properties				
			$\bar{D}_{EM}$ (nm)	$\bar{D}_{SAXS}$ (nm)	t (nm)	f	S/N (nm^2)
L-1	21	53	17	17.2	2.0±0.2	0.23	4.1
L-2	31	40	24	25.1	1.7±0.2	0.14	4.2
L-3	49	45	28	32.0	1.9±0.2	0.12	5.2
L-4*	55	46	34	34.1	2.3±0.2	0.13	5.4
L-5*	97	51	46	46.4	2.6±0.2	0.11	7.1
L-6	102	61	51	50.4	1.7±0.2	0.067	6.8

* Polymerized by slightly different procedures from the others.

polymers having lamellar microdomains. The specimens were synthesized by anionic polymerization, using sec-BuLi as an initiator and tetrahydrofuran as a polymerization medium. The samples L-1 to L-3 and L-6 were polymerized by a sequential polymerization of the monomers, while the specimens L-4 and L-5 (designated as "simultaneously polymerized materials" for convenience) were prepared by polymerizing first 50 wt % of all styrene monomers, followed by a simultaneous copolymerization of residual 50 wt % styrene monomers and all isoprene monomers. The microstructure of polyisoprene was estimated to be 38, 59, and 3 %, 1, 2-, 3, 4-, and 1, 4-additions, respectively[32].

The spacings as estimated by electron microscopy ($\bar{D}_{EM}$) and SAXS ($\bar{D}_{SAXS}$) systematically increase with increasing molecular weight. On the other hand the thickness of the diffuse-boundary t, as will be described in section V, is almost constant at about 2 nm. Thus, the volume fraction of the interfacial region $f(=2t/\bar{D})$ systematically decreases with increasing molecular weight. This evidence is necessary to understand some physical properties of such heterophase systems[22-38].

The interfacial area (S/N) occupied by a block polymer chain can be estimated from the domain spacing $\bar{D}$ and the molecular volumes of PS (v_S) and PI block (v_I) sequences:

$$S/N = 2(v_S+v_I)/\bar{D} \tag{10}$$

The area also increases with increasing molecular weight as expected.

Figure 21 shows a schematic diagram of the packing of chain molecules in the domain space. For the polystyrene domain of the L-6 specimen, for example, it turns out in the context of the confined chain-statistics that the root mean squared end-to-end distances projected on to the x, y and z-directions are

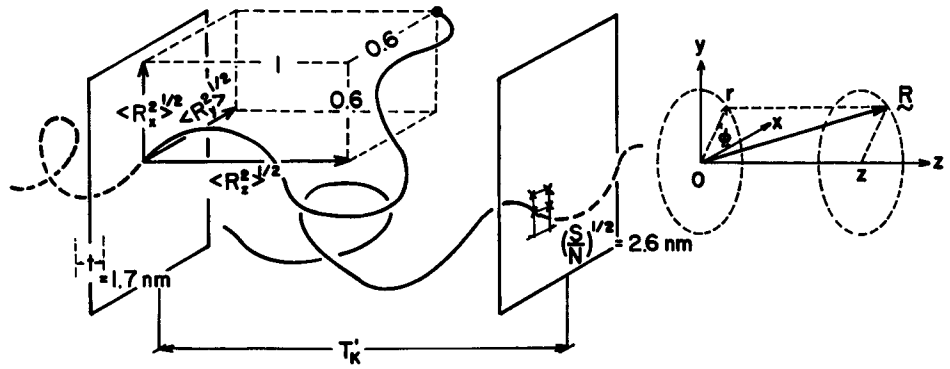

Fig. 21. Schematic diagram showing packing of chain molecules in the domain space. The values indicated in the figure are for the polystyrene lamella for L-6 specimen in Table II. The fact that $\langle R_z^2\rangle^{1/2}/\langle R_x^2\rangle^{1/2}=1.7$ indicates that the chain in domain space is expanded along the lamellar normal. The nearest neighbour distance between the two chemical junction points is much smaller (about 1/4) than the $\langle R_x^2\rangle^{1/2}=\langle R_y^2\rangle^{1/2}$, indicating that the neighbouring molecules are heavily overlapped and interpenetrated to result in uniform filling of the space. (Hashimoto, Shibayama, and Kawai, 1980).

$$\langle R_x^2\rangle^{1/2} = \langle R_y^2\rangle^{1/2} = 9.6 \text{ (nm)}$$
$$\langle R_z^2\rangle^{1/2} = 16.4 \text{ (nm)} \simeq T_{PS}'/2 \tag{11}$$

where T_{PS}' is the distance between the "walls"[23]. The confined chain statistics are based upon the random-flight statistics in the restricted volume under the constraint of the uniform volume-filling.

Thus the ratio $\langle R_z^2\rangle^{1/2}/\langle R_x^2\rangle^{1/2}=1.70$, indicating that the chain in the domain space is expanded along the lamellar normal. The nearest-neighbour distance between the two chemical junction points along the interface is approximately $(S/N)^{1/2}=2.6$ nm, roughly equal to the interfacial thickness, 1.7 nm. This distance $(S/N)^{1/2}$ is much smaller than $\langle R_x^2\rangle^{1/2}=\langle R_y^2\rangle^{1/2}$, indicating that the neighbouring molecules are heavily overlapped and interpenetrated to result in a uniform filling of the space.

Figure 22 shows the measured domain spacing $\bar{D}$ and the interfacial thickness t as functions of the total molecular weight of the block polymers[23]. The straight line in the plot of $\bar{D}$ vs. $\bar{M}n$ has a slope of 2/3 and gives an empirical relationship,

$$\bar{D} = 0.024\, \bar{M}n^{2/3} \text{ (nm)} \tag{12}$$

The power 2/3 is substantially greater than the 1/2 power expected for the molecular-weight dependence of the unperturbed chain-dimensions. This indicates that the chain in the domain-space expands due to the constraint volume effect (A and B chains being restrctied to A and B domains, respectively), and to the chain

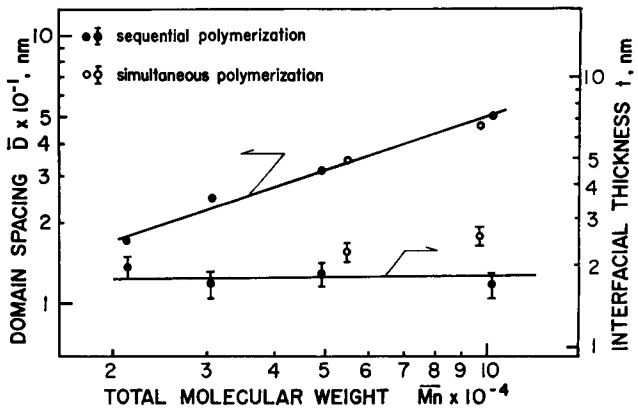

Fig. 22. Measured domain spacing $\bar{D}$ and the interfacial thickness t as a function of total molecular weight for the series of the block polymers shown in Table II. The straight line in the plot of log $\bar{D}$ vs. log $\bar{M}n$ has a slope of 2/3. (Hashimoto, Shibayama, and Kawai, 1980).

perturbations required to maintain uniform segment density in the domain. This chain-expansion depends on molecular weight, thus giving rise to a power greater than 1/2.

It should be noted that the $\bar{D}$-values for the polymers prepared by the simultaneous copolymerization fall into the same trend as those for the polymers prepared by the sequential polymerization. This should be due to the fact that the reaction rate of styrene is much faster than that of isoprene in tetrahydrofuran medium, so that the copolymerization may result in almost the same primary structure as the one prepared by the sequential polymerization.

From eqs. (10) and (12), the interfacial area S/N turns out to increase with increasing molecular weight,

$$S/N = 0.14\ \bar{M}n^{1/3}\ (\mathrm{nm}^2) \tag{13}$$

It should be worthy of note that the chemical junction points of the block polymers occupy a very minor portion of the interfaces. A majority of the interfaces is occupied by the polystyrene and polyisoprene segments, which are not covalently bonded but rather weakly bonded by van der Waals force across the interface as in the case of polymer blends. This tendency is enhanced with increasing molecular weight, and in the limiting case of infinitely large molecular weight the block polymer interfaces become identical to the interfaces of polymer blends.

Table III summarizes the interdomain distance $\bar{D}$, the average radius of the domain $\bar{R}$, the parameter related to polydispersity of the domain size $\sigma_r/\bar{R}$, the

Table 3. Domain and Domain-Boundary Properties of Spherical Microdomains (Hashimoto, Fujimura and Kawai, 1980)

Specimen Code	$\bar{M}n \times 10^{-4}$		PI-Block	Domain			Domain-Boundary			
	Total	PI-Block		$\bar{D}$ (nm)	$\bar{R}$ (nm)	σ_r/R	ΔR (nm)	$\Delta R/\bar{R}$	f	S/N (nm^2)
SI-1	8.0	1.3	16.0	24.1	6.6	0.15	2.0	0.30	0.19	10.6
SI-2	14.5	2.0	13.9	30.4	8.0	0.15	1.7	0.21	0.11	13.5
SI-3	20.2	2.6	12.9	33.9	9.4	0.11	1.7	0.18	0.085	14.9
SI-4	21.9	3.4	15.4	40.4	12.7	0.09	2.1	0.17	0.093	14.4
SI-5	32.2	7.1	21.9	66.2	17.1	0.10	2.0	0.12	0.095	22.3
SI-6	65.7	14.4	21.9	109.0	31.0	0.10	(1.5)	(0.05)	0.033	25.0

interfacial thickness ΔR, the relative interfacial thickness $\Delta R/\bar{R}$ and the overall volume fraction of the interfacial regions f and the interfacial area (S/N) occupied by a block polymer chain for the series of the S-I diblock polymers having the spherical polyisoprene domains dispersed in the matrix of polystyrene. The diblock polymers were all prepared by the same sequential polymerization technique as in the polymers in Table II.

As in the lamellar domain system, the average size of the spheres, inter-sphere distances and S/N systematically increases with increasing the molecular weight of the block polymers. The interfacial thickness is again almost independent of the molecular weight covered in this work (about 2 nm). This again results in decreasing the interfacial volume fraction with increasing the molecular weight.

$$\bar{R} \sim \bar{M}n^{2/3}, \quad \bar{D} \sim \bar{M}n^{2/3}, \quad S/N \sim \bar{M}n^{1/3} \tag{14}$$

These results will be discussed in detail in the following section.

IV-4. Equilibrium and Non-equilibrium Aspects of the Microdomains

In this section we shall compare the experimental results discussed in the preceding section with those predicted from the equilibrium theories as discussed in section III. For these comparisons, one needs to know Kuhn's statistical segment lengths b_{PS} and b_{PI} for PS and PI, respectively, the number density of monomeric units ρ_{0S} and ρ_{0I} for the respective polymers and the interaction parameter α.

As for the statistical segment length b_{PS}, we shall use the value reported by Ballard, Wignall and Schelten[39] on neutron scattering experiments for bulk polystyrene,

$$b_{PS} = 0.68 \text{ (nm)}$$

For polyisoprene having a cis-1,4-configuration we shall adopt the value listed in the Polymer Handbook[40], while for polyisoprene having a high vinyl content as

listed in Tables II and III, we shall adopt the value estimated from the measurements of intrinsic viscosity at θ-temperature (57.1°C in ethylacetate)[32].

$b_{PI} = 0.59$ (nm) for the polymers in Tables II and III
$b_{PI} = 0.67$ (nm) for cis-1, 4-polyisoprene

The density of pure polymers were measured by the density gradient tube method,

$$\rho_{0PS} = 1.01 \times 10^4, \quad \rho_{0PI} = 1.36 \times 10^4 \text{ (mol/m}^3\text{)}$$

As for the parameter α we shall adopt a value at room temperature, according to the formula obtained by Rounds and McIntyre as cited in the work of Helfand[14],

$$\alpha = -900 + 7.5 \times 10^5 / T \text{ (mol/m}^3\text{)} \tag{15}$$

It should be noted that this result was obtained for cis-1,4-polysioprene, and is not strictly applicable to the interaction with the polyisoprene having a high vinyl content.

Figure 23 shows the average lamellar spacings $\bar{D}$ plotted as a function of the total molecular weights for various block polymers having lamellar morphology such as

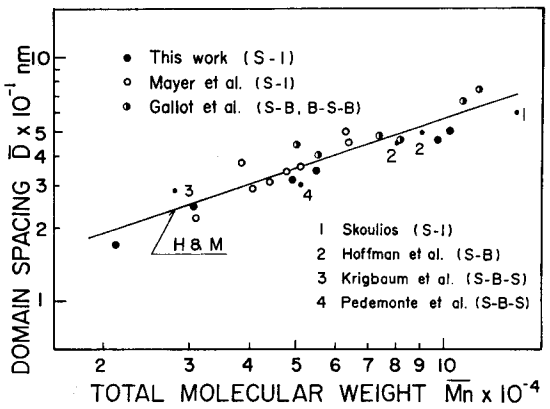

Fig. 23. The average lamellar spacing $\bar{D}$ plotted as a function of total molecular weight for various block polymers having lamellar morphology. S-I, S-B, B-S-B, and S-B-S stand for the usual meaning (S, I and B referring to polystyrene, polyisoprene, and polybutadiene block chains). The solid line is the result predicted from Helfand and Meier's theories for the diblock polymers having equal block molecular weights and having the parameters as described in the text. The triblock polymers S-B-S and B-S-B are replaced by the diblock polymers having S-(1/2)B and B-(1/2)S, respectively. (Hashimoto, Shibayama, and Kawai, 1980).

S-I and S-B diblock polymers, B-S-B and S-B-S triblock polymers[23]. The experimental results were obtained by many groups; Mayer et al.[41,42] (large open circles), Gallot et al.[2,42,43] (large half-filled circles), this work shown in Table II[23] (large filled circles), Skoulios[3] (small solid circle numbered 1), Hoffmann et al.[4] (small solid circles numbered 2), Krigbaum et al[21]. (small solid circle numbered 3) and Pedemonte at al.[44] (small solid circle numbered 4). The solid line is the result predicted from Helfand and Meier's theories for the diblock polymers having equal molecular weights for the two blocks and having the parameters as described earlier[23], the statistical segment length of polybutadiene b_{PB} being assumed to be $b_{PB}=b_{PI}=0.59$. It is also assumed that $\rho_{0PB}=\rho_{0PI}$ and that the interaction parameter α for polystyrene and polybutadiene is also given by eq. (15). It should be noted that the morphology of the triblock polymers S-B-S and B-S-B is approximately equal to that of the diblock polymers S-(1/2)B and B-(1/2)S, respectively, the relation of which is used in the plot of Figure 23.

The general trend is that the spacings predicted from both Helfand and Meier's theories are almost identical and agree also with the experimental results. This may indicate that the size of the lamellar microdomain is predictable by the equilibrium theories and therefore by the molecular and thermodynamic parameters such as Z_K, ρ_{0K}, b_K and α. Also, the global conformation of the chain molecules in the domain space can essentially be described by the random flight chain statistics. Some scattering of data points may be primarily due to a difference in chemical composition and the microstructure for each polymer. It should be pointed out that the spacings for the polymers having a high content of cis-1,4-polyisoprene are slightly larger (by about 7 %) than those for the polymers having a high vinyl content, since the segment length of the former is larger than that of the latter.

Figure 24 shows the average domain radius $\bar{R}$ as a function of the molecular weight of polyisoprene block forming the spherical domains (a) and the interdomain distance $\bar{D}$ as a function of the total molecular weight (b) for a series of block polymers having a spherical polyisoprene domain dispersed in polystyrene matrix (Table III)[31]. The solid lines are the measured results, and the broken lines marked H are the results calculated from the theory of Helfand and Wasserman[16].

It is interesting to note that the absolute values of experimental $\bar{R}$ and $\bar{D}$ are about 1/2 of the theoretical values. Moreover, despite the large discrepancy in the absolute values, their relative molecular-weight dependences are almost identical. This tendency is a big contrast to the lamellar domain system in which was found almost complete agreement between the theoretical and experimental results

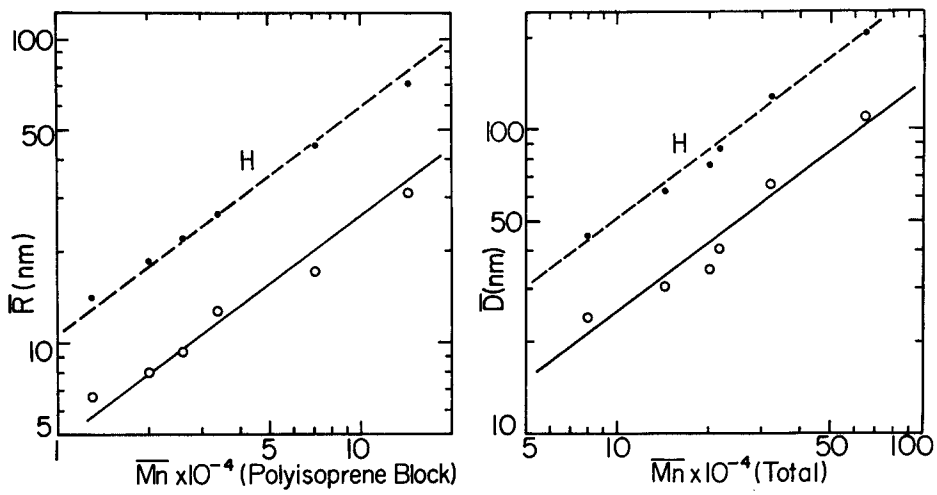

Fig. 24. (a) Average domain radius $\bar{R}$ as a function of molecular weight of polyisoprene block forming the sphere and (b) the interdomain distance $\bar{D}$ as a function of total molecular weight for the series of the block polymers having spherical polyisoprene domain dispersed in matrix of polystyrene (see Table III). The solid lines are the measured results and the broken lines marked H are the results calculated from the theory of Helfand and Wasserman. (Hashimoto, Fujimura, and Kawai, 1980).

in terms of both absolute values and relative molecular-weight dependences.

This discrepancy may be attributed to a non-equilibrium effect encountered in the solvent evaporation process. The domain structure will be fixed when the solvent content falls to such a value that the polystyrene glass transition temperature is the solvent evaporation temperature (i.e., at the concentration C_3^* in Figure 2). The solvent is further removed but the system cannot reach equilibrium.

The radius R_A and interdomain distance D of the spherical domain are related to the molecular volumes v_A and v_B, and the number of block polymer chains per one domain N,

$$4\pi R_A^3/3 = Nv_A \tag{16}$$

$$D^3/\sqrt{2} = N(v_A+v_B) \tag{17}$$

where in eq. (17) the sperical domains are assumed to be arranged in a hexagonal closed pack. A possible interpretation for the discrepancy of the absolute values of D and R_A is that the number N in the real system is much less than the equilibrium value. During the solvent evaporation, the systems attain new equilibrium by changing the domain size, i.e., by changing N. The lamellar or cylindrical domains can change their sizes or the number N simply by shrinking along the interface, i.e., by decreasing the distance between adjacent chemical junction points along the interface.

On the other hand the spherical domain can change its size only by a process involving the transport of $A(B)$-chains through the matrix of $B(A)$-chains. This process must overcome a larger energetic barrier than that involved in the lamellar or cylindrical domains. This must be a main reason why the non-equilibrium effect of the spherical domain system is large compared with that of the lamellar system. This energetic barrier increases with increasing concentration for a given solvent polymer combination and the molecular weight. However, the conformation of the chain within the domain may be close to the equilibrium. Thus, the observed values of $\bar{D}$ and $\bar{R}$ may reflect the equilibrium values relevant at some concentrations but not at 100 % polymer. Consequently, the relative molecular-weight dependences are close to those calculated from the equilibrium theory,

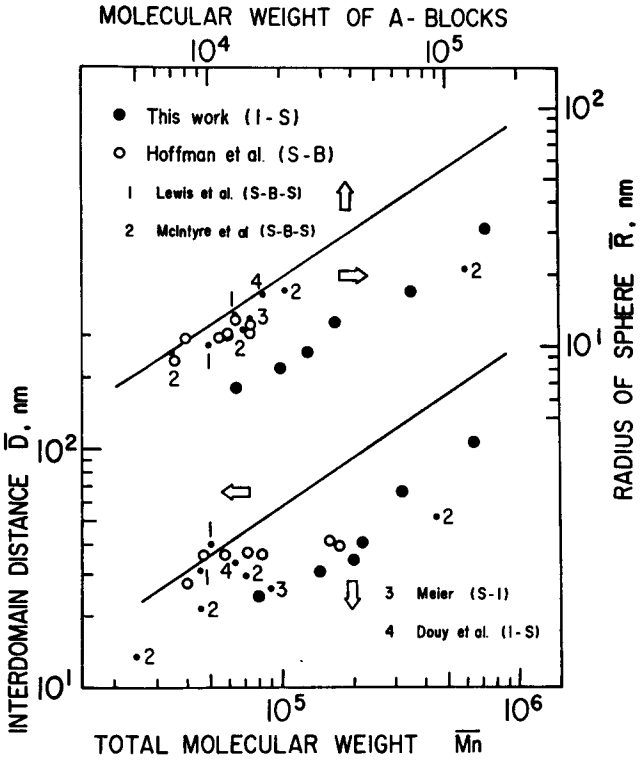

Fig. 25. Average interdomain distance $\bar{D}$ as a function of total molecular weight and the radius $\bar{R}$ as a function of molecular weight of the block chain forming the sphere for various block polymers having spherical morphology. The first letter I of I-S stands for the polyisoprene block chain forming the sphere. The solid lines are calculated from the theory of Helfand and Wasserman for the block polymers with 20 wt % polyisoprene or polybutadiene. (Hashimoto, Fujimura, and Kawai, 1980).

but their absolute values are far below the theoretical values. The real spherical domains systems in solid state are in a metastable state which has an excess interfacial area, interfacial volume and therefore excess free energy.

Figure 25 shows the distance $\bar{D}$ as a function of the total molecular weight and the radius $\bar{R}$ as a function of the molecular weight of the block chain forming the sphere for various block polymers having spherical morphology. The symbols I-S, S-B, and S-B-S stand for the usual meaning, and the first letter I of I-S stands for the block chain forming the sphere. In the figure are included our data[31] shown in Table III (large solid circles), data by Hoffmann and co-workers[4] (large open circles), Lewis and Price[45] (small solid circles numbered 1), McIntyre and co-workers[46] (small solid circles nimbered 2), Meier[11] (small solid circles numbered 3) and Douy et al.[42] (small solid circles numbered 4). The solid lines are calculated from the theory of Helfand and Wasserman[16] for the same molecular and thermodynamic parameters as in the calculation of the lamellar microdomains and the composition having 20 wt % polyisoprene.

A general trend is that the non-equilibrium effect is remarkable for the spherical domain systems, giving rise to observed values generally smaller than the calculated values. Only those polymers having very low molecular weight and high polyisoprene or polybutadiene content closely follow the predicted behavior in terms of both $\bar{D}$ and $\bar{R}$.

V. Polymer-polymer Interphase in Block Polymers

V-1. Earlier Works

The evaluation of the domain-boundary interphase of the block polymers and polymer blends are still very challenging experimental problems, and only a very limited number of works have been reported so far. The SAXS scattering method is the most powerful method to evaluate the interfacial thickness.

One way to evaluate the interfacial thickness is the analyses of the invariant Q, the integrated intensity of SAXS overall reciprocal space,

$$Q = \int_0^\infty I_s(h)h^2dh = 2\pi^2 I_e V\langle\eta^2\rangle \tag{18}$$

$$h = 2\pi s = (4\pi/\lambda)\sin\theta$$

The invariant is related to the mean square electron density variation of the system[47]. The scattered intensity $I_s(h)$ is corrected for the slit-smearing effects and the background scattering I_e is the Thomson scattering intensity for an electron. For an ideal two-phase system with electron density ρ_i and volume fraction ϕ_i for i-th phase ($i=1,2$), it follows that

$$\langle \eta^2 \rangle = \phi_1 \phi_2 (\rho_1 - \rho_2)^2 \tag{19}$$

For a pseudo two-phase system having a trapezoidal electron density variation as in Figure 26[48],

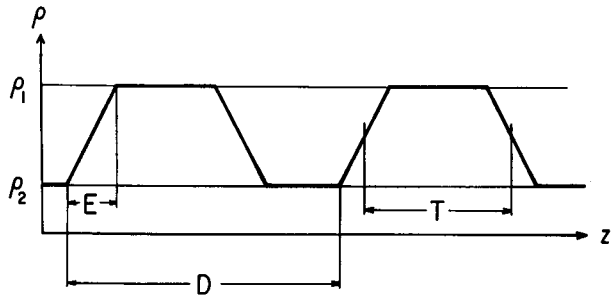

Fig. 26. A pseudo two-phase system having trapezoidal electron density variation.

$$\langle \eta^2 \rangle = \left(\phi_1 \phi_2 - \frac{1}{6} \phi_3 \right) (\rho_1 - \rho_2)^2 \tag{20}$$

$$\phi_3 = SE/V$$

Thus the decrease of $\langle \eta^2 \rangle$ and therefore of the intensity from those expected for the ideal two-phase systems are the measure of the interfacial volume fraction ϕ_3 and the interfacial thickness E. (S being the total interfacial area of the system.)

The principle was first applied by LeGrand[49] to estimate the interfacial volumes of S-B-S and S-I-S triblock polymers. He concluded the diffuse boundary. Later, a similar analysis was made by Kim[50] for the S-B-S polymer with a trade name of Kraton 101 who concluded a sharp boundary contrary to the conclusion made by LeGrand. In either case, only the arguments of the type of "all" or "none" were made at that stage.

In the cases of lamellar microdomains, the particle factor at the N-th order scattering maximum $I_p(N)$, on the basis of the one-dimensional paracrystalline analysis made by Hosemann and Bagchi,[51] is given by

$$I_p(N) = \left[\frac{\sin N\pi\phi}{N\pi\phi} \frac{\sin N\pi\phi(E/T)}{N\pi\phi(E/T)} \right]^2 \tag{21}$$

where

$$2D \sin\theta = N\lambda\,, \quad \phi = T/D \tag{22}$$

Skoulios and his co-workers[3] utilized this relation and estimated $E \simeq 1.2$ nm from the measured intensity ratio of the 15th-order to the first-order scattering maximum for a particular S-I diblock polymer having a total molecular weight of 3×10^5 g/mol,

$\bar{D}$=90 nm and ϕ=0.5. Consequently, they concluded a sharp interphase.

Hashimoto and his co-workers[27] also made a paracrystalline analysis for a particular S-I diblock polymer having a total molecular weight 1.05×10^5 and a lamellar morphology. They obtained the value E approximately twice as large as the value obtained by Skoulios and his co-workers. Therefore, this is still a controversial subject and obviously a more quantitative analysis is required.

V-2. Analysis of SAXS Profiles in the Large Scattering Angles

A quantitative way to analyze the thickness of the diffuse boundary is proposed by Vonk[48] and Ruland[52], and first applied by Vonk[48]. This method is based on an analysis of the systematic deviation of the SAXS intensity distribution at the large angle tail from Porod's rule[53] established for the ideal two-phase system.

The electron density variation $\eta(\boldsymbol{r})$ for a pseudo two-phase system is given by a convolution product of the electron density variation of the ideal two-phase system $\rho(\boldsymbol{r})$ and a smoothing function $h(\boldsymbol{r})$ related to the interfacial thickness,

$$\eta(\boldsymbol{r}) = \rho(\boldsymbol{r})*h(\boldsymbol{r}) = \int d\boldsymbol{u}\,\rho(\boldsymbol{u})h(\boldsymbol{r}-\boldsymbol{u}) \tag{23}$$

The scattered intensity from such a system is then given by

$$I(s) = \mathcal{F}\{\overset{2}{\tilde{\eta}}(\boldsymbol{r})\} \equiv \int d\boldsymbol{r}\,\overset{2}{\tilde{\eta}}(\boldsymbol{r})\exp(2\pi i\boldsymbol{s}\cdot\boldsymbol{r}) \tag{24}$$

$$= I_g(\boldsymbol{s})I_h(\boldsymbol{s}) \tag{25}$$

where

$$I_g(\boldsymbol{s}) = \mathcal{F}\{\overset{2}{\tilde{\rho}}(\boldsymbol{r})\} \tag{26}$$

which is given for an isotropic system by

$$I_g(s) = [(2\pi)^{-3}I_e(\rho_1-\rho_2)^2S]s^{-4}\ \text{(Porod's rule)} \tag{27}$$

where S is the total interfacial area. $\overset{2}{\tilde{\eta}}$ is the self-convolution of the function η defined by

$$\overset{2}{\tilde{\eta}}(\boldsymbol{r}) = \int d\boldsymbol{u}\,\eta(\boldsymbol{u})\eta(\boldsymbol{r}+\boldsymbol{u})$$

For a spherical domain system, $h(\boldsymbol{r})$ depends only on r, while for a cylindrical or lamellar domain system, the boundary exists in a radial direction or in a direction parallel to the lamellar normal. If the function $h(r)$ may be approximated by Gaussian, i.e.,

$$h(r) = (2\pi\sigma^2)^{-3/2} \exp(-3r^2/2\sigma_3^2) \text{ (for spherical domain)}$$
$$= (2\pi\sigma^2)^{-1} \exp(-2r^2/2\sigma_2^2) \text{ (for cylindrical domain)}$$
$$= (2\pi\sigma^2)^{-1/2} \exp(-r^2/2\sigma_1^2) \text{ (for lamellar domain)} \quad (28)$$

then it can be shown that

$$I_h(s) = \exp(-4\pi^2\sigma^2 s^2), \quad \sigma^2 \equiv \sigma_j^2/j \qquad (j = 1, 2, 3) \quad (29)$$

for all domain shapes where σ is the parameter characterizing the interfacial thickness.

Thus, for the spherical domain systems or for the cylindrical or lamellar domain systems in which the cylinders or lamellae are randomly oriented, the scattering intensity is given by

$$I(s) = Cs^{-4} \exp(-4\pi^2\sigma^2 s^2) \quad (30)$$
$$C = (2\pi)^{-3} I_e (\rho_1 - \rho_2)^2 S$$

Consequently, a plot of $\ln s^4 I(s)$ *vs.* s^2 yields the parameter σ. It should be noted that the intensity $I(s)$ is corrected for the slit-smearing effects and the background scattering arising from the local atomic order within each phase.

If the cylinders or lamellae have a macroscopic orientation, one has to take into account this orientation effect. For example, for perfectly oriented lamellar systems the scattered intensity $I(s)$ along the lamellar normal is given by[26]

$$I(s) \sim s^{-2} \exp(-4\pi^2\sigma^2 s^2) \quad (31)$$

Thus, in this case a plot of $\ln s^2 I(s)$ *vs.* s^2 yields a parameter σ.

The Gaussian smoothing function $h(r)$ in eq. (28) gives a smooth sigmoidal electron density variation in the interphase. It can be shown that $\eta(r)$ near the interphase is given for spherical domains[31]

$$\eta_s(r) = \pi^{-1/2}\rho_0 \left\{ Erf\left(\frac{r+R}{\sqrt{2}\sigma}\right) + \frac{\sigma}{\sqrt{2}r} \exp\left[-\left(\frac{r+R}{\sqrt{2}\sigma}\right)^2\right] \right.$$
$$\left. - Erf\left(\frac{r-R}{\sqrt{2}\sigma}\right) + \frac{\sigma}{\sqrt{2}r} \exp\left[-\left(\frac{r-R}{\sqrt{2}\sigma}\right)^2\right] \right\} \quad (32)$$

for lamellar domains[23],

$$\eta_l(r) = \pi^{-1/2}\rho_0 \left\{ Erf\left(\frac{Z+a}{\sqrt{2}\sigma}\right) - Erf\left(\frac{Z-a}{\sqrt{2}\sigma}\right) \right\} \quad (33)$$

for cylindrical domains

$$\eta_c(r) = (2\pi\sigma^2)^{-1}\rho_0 \int_0^R x dx \exp[-(r^2+x^2)] \int_0^{2\pi} d\phi \cosh[(rx/2\sigma^2)\cos\phi] \quad (34)$$

where $a=T/2$ (T being defined in Figure 26), ρ_0 is the electron density difference between the two-phases, and $Erf(x)$ is the error function defined as

$$Erf(x) = \int_0^x dt \exp(-t^2)$$

Figure 27 shows a typical electron density profile for the spherical domain which is given by eq.(23). One can define the interfacial thickness ΔR for the

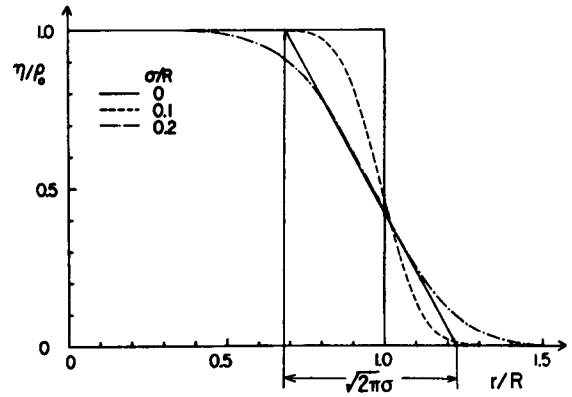

Fig. 27. A typical electron density profile for a spherical domain system which is given by a convolution product of the step function with the Gaussian smoothing function. (See eq. (23) or (32) in the text.) (Hashimoto, Fujimura, and Kawai, 1980).

spherical domain, and t for the lamellar domain corresponding to the system having a linear density transition in the interphase.

$$\begin{aligned} \Delta R &\equiv \rho_0 / |d\eta_s(r)/dr|_{r=R} \simeq \sqrt{2\pi}\,\sigma \\ t &= \rho_0 / |d\eta_l(r)/dr|_{r=a} \simeq \sqrt{2\pi}\,\sigma \end{aligned} \tag{35}$$

It should be noted that ΔR and t are the minimum estimations of the interfacial thickness.

It is necessary to understand some effects of waviness in the interface and of the size distributions of the domain on the estimated interfacial thickness. In principle, the surface waviness and size distribution do not affect the interfacial thickness if the wavelength of the surface waviness is much larger than the interfacial thickness and if the size distribution of the domains is narrow enough so that the domains having their sizes comparable to the interfacial thickness make negligible contribution to the total scattering. These conditions are usually satisfied in such block polymer systems as we are discussing in this text. Generally,

the surface waviness and size distribution affect the proportional constant C in in eq.(30) and push Porod's law region toward higher scattering angles.

V-3. Some Results on Spherical and Lamellar Microdomains

Figure 28 shows a typical SAXS curve at the large angle tail for a particular specimen L-6 in Table II, having lamellar microdomains which have almost the perfect orientation as discussed in section IV-2[23]. The desmeared intensity was

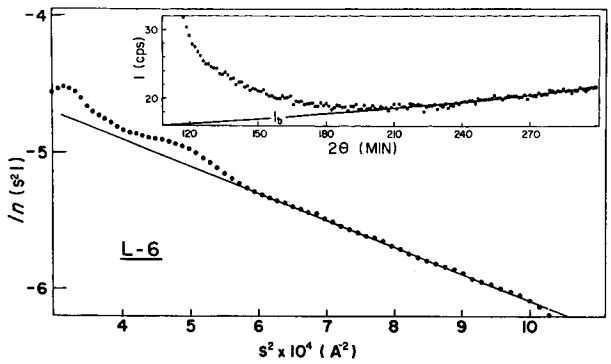

Fig. 28. A typical SAXS curve at large scattring angle for a particular specimen L-6 in Table II and the background scattering I_b. The intensity I corrected for the background scattering is used in the plot of ln $s^2I(s)$ vs. s^2 to estimate the interfacial thickness σ or $t=\sqrt{2\pi}\sigma$ (see eq. (31) in the text). (Hashimoto, Shibayama, and Kawai, 1980).

corrected for the background scattering I_b, which was empirically estimated by a nonlinear curve fitting of the scattering profile over a sufficient large angular lange with the polynomials or the Gaussian functions as proposed by Vonk[48] and Ruland[54]. The intensity corrected for the background scattering was then plotted as shown in the figure to estimate σ. The interfacial thickness t thus evaluated is summarized in Table II.

Figure 29 shows typical plots to estimate σ for a particular specimen SI-5 in Table III having spherical microdomains[31]. The plot of ln s^4I vs. s^2 directly gives the value σ from the slope of the straight line. However, this plot requires the desmearing of the measured intensity profile. This desmearing of the curve in the large angle tail generally involves great difficultities caused by a severe amplification of the statistical errors of data and is not always possible for some systems[55]. The difficulties may be circumvented by evaluating σ by a nonlinear curve fitting of the smeared data[31] (in the plot of ln $s^3\tilde{I}$ vs. s^2) with the smeared theoretical intensity $\tilde{I}_{\text{theor.}}$. (ln $s^3\tilde{I}_{\text{theor.}}$ vs. s^2).

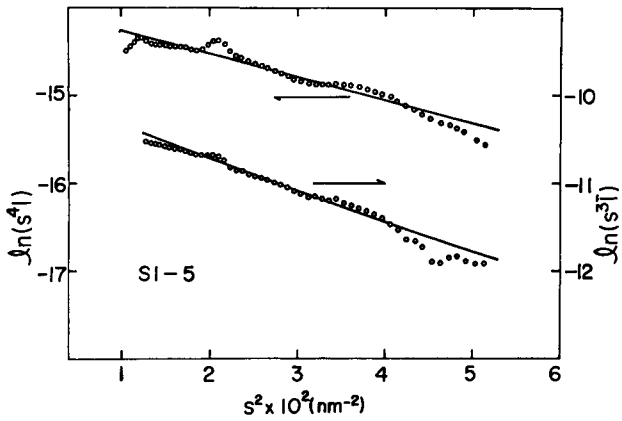

Fig. 29. Typical plots of $\ln s^4 I(s)$ vs. s^2 or $\ln s^3\tilde{I}(s)$ vs. s^2 to estimate or $\Delta R=\sqrt{2\pi}\sigma$ for a particular specimen SI-5 in Table III having spherical microdomains. The plot of $\ln s^4 I(s)$ vs. s^2, which is based on the desmeared intensity, directly gives the value σ from the slope of the straight line. The plot of $\ln s^3\tilde{I}(s)$ vs. s^2, which is based on the smeared intensity, gives the value σ by a nonlinear curve fitting of the smeared data ($\ln s^3\tilde{I}$) with the smeared theoretical intensity ($\ln s^3\tilde{I}_{theor}$).

$$\tilde{I}_{\text{theor.}}(s) = \int_{-\infty}^{\infty} W_l(u) I(\sqrt{s^2+u^2})\, du \tag{36}$$

where $W_l(u)$ is the slit-length weighting function which is measured or calculated for a given optical system and $I(s)$ is given by eq. (30). The two types of plots were confirmed to yield identical results. This detailed procedure will be described elsewhere[31]. The interfacial thickness ΔR thus evaluated is summarized in Table III.

As shown in Table IV and V and also in Figure 22, the interfacial thickness

Table 4. Comparison of Measured and Predicted Domain-Boundary Thicknesses of Lamellar Domain Systems (Hashimoto, Shibayama, and Kawai, 1980)

Sample Code	total $\bar{M}n\times10^{-3}$	wt % of PS	Interfacial Thickness t, nm		
			SAXS	Meier	Helfand
L-1	21	53	2.0±0.2	3.4	1.4
L-2	31	40	1.7±0.2	3.4	1.4
L-3	49	45	1.9±0.2	3.3	1.4
L-4*	55	46	2.3±0.2	3.2	1.4
L-5*	97	51	2.6±0.2	2.8	1.4
L-6	102	61	1.7±0.2	2.8	1.4

* Polymerized with slightly different procedure

Table 5. Comparison of Measured and Predicted Domain-Boundary Thicknesses of Spherical Domain Systems (Hashimoto, Fujimura, and Kawai, 1980)

Specimen	$Mn\times10^{-3}$ PS/PI	ΔR (nm)		$\Delta R/\bar{R}$		
		Exptl.	Calcd.[a)]	Exptl.	H[b)]	M[c)]
SI-1	67/13	2.0±0.1	1.60	0.30	0.105	0.30
SI-2	125/20	1.7±0.1	1.60	0.21	0.074	0.18
SI-3	174/26	1.7±0.2	1.60	0.18	0.094	0.14
SI-4	186/34	2.1±0.2	1.60	0.17	0.052	0.11
SI-5	249/71	2.0±0.1	1.60	0.12	0.031	0.05
SI-6	520/140	1.5±0.2	1.60	0.048	0.019	0.03

a) Helfand & Sapse, J. Chem. Phys., **62**, 1327 (1975),
$\Delta R=2\left[\frac{\beta_A^2+\beta_B^2}{2\alpha}\right]^{1/2}$, $\beta_K^2=\frac{1}{6}\rho_{0K}b_K^2$

b) Helfand & Wasserman, Macromolecules, **11**, 966 (1978).

c) Meier, in "Block & Graft Copolymers," 1973.

is not a strong function of molecular weights covered in this work. In the case of the lamellar domain system it turns out that the thickness t for the polymers prepared by the simultaneous polymerization is slightly but significantly larger than that of the polymers prepared by the sequential polymerization. Thus, a slight perturbation of the primary structure caused by a mixing of styrene and isoprene monomers near the chemical junction point between PS and PI enhances the mixing of the incompatible segments to result in the increased interfacial thickness.

Table IV and V also include the interfacial thickness calculated from the theories of Meier and Helfand-Wasserman[15,16]. The interfacial thickness calculated from the theory of Helfand-Wasserman is a constant 1.4 nm for the lamellae and 1.6 nm for the spheres, indepent of molecular weight. This is a consequence of invoking the narrow interphase approximation[14]. On the other hand, the interfacial thickness of the lamellar microdomains calculated from Meier's theory depends on molecular weight, decreasing with increasing molecular weight, approximately according to $M^{-1/3}$, to an asymptotic value of the Debye interaction range parmeter[56] ($\sim$0.8 nm). Thus in the limit of infinite molecular weight, Helfand's interfacial thickness is much larger than Meier's interfacial thickness.

Although there are some discrepancies between the measured and calculated interfacial thicknesses, we may conclude that the agreement is fairly good and that the discrepancies are within the errors involved in estimating the interaction parameter α at the present stage. In this regard it is essential to obtain an accurate value of α to distinguish the theories.

Table VI summarizes the temperature-dependence of the interfacial thickness for a particular specimen SI-3 having the spherical domain[57]. The measured

Table 6. Domain-Boundary Properties of Spherical Domains (Fujimura et al., 1980)

Temperature (°C)	Observed Values		Theoretical Values	
	$\Delta R/R$	ΔR (nm)	$\Delta R/R$*)	ΔR (nm)**)
20	0.15	1.4±0.15	0.15	1.37
173	0.19	2.2±0.15	0.31	2.00

*) Meier $\Delta R/R=8/\chi_{AB}$, $\chi_{AB}=\alpha Z/\rho_0$
**) Halfand $\Delta R=2[(\beta_A{}^2+\beta_B{}^2)/2\alpha]^{1/2}$
$\alpha=(\delta_A-\delta_B)^2/k_BT=-900+7.5\times10^5/T$ (mol/m^3) (N.A. Rounds & D. McIntyre)

interfacial thickness increases by about 60 % with an increasing temperature up to 173°C. This increase is predictable in terms of the temperature dependence of the interaction parameter α as shown in the calculated values of ΔR based on the theory of Helfand-Sapse[22]. With an increasing temperature, the interaction parameter α decreases and therefore the interfacial thickness increases. The temperature 173°C is still far below the critical temperature T_c which is expected to be above 300°C as discussed in section III-2. Therefore, this temperature does not significantly affect the domain and domain-boundary structure yet. The change of the domain structure at a temperature near T_c is one of the most important subjects to be clarified, a part of the work being presented elsewhere[7].

Acknowledgement

A part of this work was supported by a Grant-in-Aid for Scientific Research from the Ministry of Education, Japan (243021 and 449012).

References

1) E. Vanzo, J. Polym. Sci., A-1, **4**, 1727 (1966).
2) C. Sadron and B. Gallot, Makromol. Chem., **164**, 301 (1973).
3) A.E. Skoulios, in "Block and Graft Copolymers", J.J. Burke and V. Weiss, Ed., Syracuse University Press, Syracuse, N.Y. (1973).
4) M. Hoffmann, G. Kämpf, H. Krömer, and G. Pampus, Adv. Chem. Ser., No. **99**, 351 (1971).
5) E.R. Pico and M.C. Williams, Polym. Eng. Sci., **17**, 573 (1977).
6) J.M. Schultz, J.S. Lin, and R.W. Hendricks, J. Appl. Cryst., **11**, 551 (1978).
7) T. Hashimoto, Y. Tsukahara, and H. Kawai, J. Polym. Sci., Polym. Letter Ed., **18**, 585 (1980).
8) T. Hashimoto, S. Suehiro, M. Shibayama, K. Saijo, and H. Kawai, Polym. J., **13**, 501 (1981).
9) G.E. Molau, in "Block Polymers", S.L. Aggarwal, ed., Plenum Press, N.Y. (1970).
10) T. Inoue, T. Soen, T. Hashimoto, and H. Kawai, Macromolecules, **3**, 87 (1970).
11) D.J. Meier, J. Polym. Sci., C**26**, 81 (1969).
12) D.J. Meier, in "Block and Graft Copolymers", J.J. Burke and V. Weiss, Ed., Syracuse University Press, N.Y. (1973).
13) D.J. Meier, Prepr. Polymer Colloquim,, Soc. Polym. Sci., Japan, Kyoto (1977) pp. 83.
14) E. Helfand, Macromolecules, **8**, 552 (1975).
15) E. Helfand and Z.R. Wasserman, Macromolecules, **9**, 879 (1976).
16) E. Helfand and Z.R. Wasserman, Macromolecules, **11**, 960 (1978).

17) T. Inoue, T. Soen, T. Hashimoto, and H. Kawai, J. Polym. Sci., A2, **7**, 1283 (1969).
18) S. Krause, J. Polym. Sci., A2, **7**, 249 (1969); Macromolecules, **3**, 84 (1970).
19) U. Bianchi, E. Pedemonte, and A. Turturro, Polymer, **11**, 268 (1970).
20) D.F. Leary and M.C. Williams, J. Polym. Sci., Polym. Phys. Ed., **11**, 345 (1973).
21) W.R. Krigbaum, S. Yazgan, and W.R. Tolbert, J. Polym. Sci., Polym. Phys. Ed., **11**, 511 (1973).
22) E. Helfand and A.M. Sapse, J. Chem. Phys., **62**, 1327 (1975).
23) T. Hashimoto, M. Shibayama, and H. Kawai, Macromolecules, **13**, 1237 (1980).
24) Y. Tsukahara, N. Nakamura, T. Hashimoto, H. Kawai, T. Nagaya, Y. Sugimura, and S. Tsuge, Polym. J., **12**, 455 (1980).
25) E. Gouinlock and R.S. Porter, Polym. Eng. Sci., **17**, 535 (1977).
26) T. Hashimoto, A. Todo, H. Itoi, and H. Kawai, Macromolecules, **11**, 377 (1977).
27) T. Hashimoto, K. Nagatoshi, A. Todo, H. Hasegawa, and H. Kawai, Macromolecules, **7**, 364 (1974).
28) M.J. Folkes and A. Keller, in "The Physics of Glassy Polymers", R.N. Haward, Ed., Appl. Sci. Publishers, London (1973).
29) J. Dlugosz, A. Keller and E. Pedemonte, Kolloid Z.u.Z., Polymere, **242**, 1125 (1970).
30) G. Kämpf, H. Krömer, and M. Hoffmann, J. Macromol. Sci-Phys., B6(1), 167 (1972).
31) T. Hashimoto, M. Fujimura, and H. Kawai, Macromolecules, **13**, 1660 (1980).
32) T. Hashimoto, N. Nakamura, M. Shibayama, A. Izumi, and H. Kawai, J. Macromol. Sci.-Phys., B**17**(**3**), 427 (1980).
33) M. Shen and D.H. Kaelble, J. Polym. Sci., B**8**, 149 (1970).
34) D.G. Fesko and N.W. Tschoegl, Intern. J. Polym. Mater., **3**, 51 (1974).
35) T. Soen, M. Shimomura, T. Uchida, and H. Kawai, Colloid & Polym. Sci., **252**, 933 (1974).
36) G. Kraus and K.W. Rollmann, J. Polym. Sci., Polym. Phys. Ed., **14**, 1133 (1976).
37) H. Odani, K. Taira, N. Nemoto, and M. Kurata, Polym. Eng. Sci., **17**, 527 (1977).
38) T. Hashimoto, M. Fujimura, K. Saijo, H. Kawai, J. Diamont, and M. Shen, Adv. Chem. Ser. No. **176**, 257 (1979).
39) D.G.H. Ballard, G.D. Wignall and J. Schelten, Eur. Polym. J., **9**, 965 (1973).
40) J. Brandrup and E.H. Immergut, ed., "Polymer Handbook", John Wiley & Sons, N.Y. (1975), Chapter IV-4.
41) R. Mayer, Polymer, **15**, 137 (1974).
42) A. Douy, R. Mayer, J. Rossi, and B. Gallot, Mol. Cryst. Liq. Cryst. **7**, 103 (1969).
43) A. Souy and B. Gallot, Makromol. Chem., **156**, 81 (1972).
44) E. Pedemonte and G.C. Alfonso, Macromolecules, **8**, 85 (1975).
45) P.R. Lewis and C. Price, Polymer, **12**, 258 (1972).
46) E. Campos-Lopez, D. McIntyre, and L.J. Fetters, Macromolecules, **6**, 415 (1973).
47) Refer for example, A. Guinier and G. Fournet, "Small-Angle Scattering of X-rays", John Wiley & Sons, Inc., N.Y. (1955).
48) C.G. Vonk, J. Appl. Cryst., **6**, 81 (1973).
49) D.G. LeGrand, J. Polym. Sci., B**8**, 195 (1970).
50) H. Kim, Macromolecules, **5**, 594 (1972).
51) R. Hosemann and S.N. Bagchi, "Direct Analysis of Diffraction by Matter", Amsterdam, North Holland (1962).
52) W. Ruland, J. Appl. Cryst., **4**, 70 (1971).
53) G. Porod, Kolloid-Z., **124**(2), 83 (1951); ibid, **125**(1), 51 (1952); ibid., **125**(2), 108 (1952).
54) J. Rathie and W. Ruland, Collid & Polym. Sci., **254**, 358 (1976).
55) A. Todo, T. Hashimoto, and H. Kawai, J. Appl. Cryst., **11**, 558 (1978).
56) P. Debye, J. Chem. Phys., **31**, 680 (1959).
57) M. Fujimura, H. Hashimoto, K. Kurahashi, T. Hashimoto, and H. Kawai, Macromolecules, in press.